System Identification of the Brompton Bicycle

A THESIS
SUBMITTED TO THE FACULTY OF THE GRADUATE SCHOOL
OF THE UNIVERSITY OF MINNESOTA
BY

Monique Victoria Teresa Hladun

IN PARTIAL FULFILLMENT OF THE REQUIREMENTS
FOR THE DEGREE OF
MASTER OF SCIENCE

Advisor: Professor Bérénice Mettler

January, 2015

Acknowledgements

I had the great privilege to work with exceptional people throughout the course of this work. I would like to thank all of them for making this experience unique and enlightening.

I would like to take the time to thank Professor Bérénice Mettler for her guidance and assistance throughout this work.

I would like to thank Professor William Garrard, Professor Demoz Gebre-Egziabher, and Professor Mihailo Jovanovic for agreeing to serve on my committee and for providing useful feedback.

I would like to thank Andrew Feit and Simon Shuster for their assistance throughout this work. I would like to acknowledge the remaining members of the team including Vishnuu Mallik, Katie Heinemann, Topher Sikorra, and Maninder Grover.

I would like to thank all of the other individuals in the *Interactive Guidance & Control Lab* who have helped the team throughout this work. I would like to acknowledge Jon Andersh, Bin Li, Kuo-Shih Tseng, and Abhishek Verma. I am thankful for all of their assistance throughout this work including taking the time to talk about new sensors, how to incorporate these devices with similar programs in the lab, and for sharing their thoughts for different approaches in order to get the work completed.

Dedication

To my family for the tremendous inspiration and support.

Abstract

The Brompton (a European folding design) bicycle was instrumented with a variety of sensors including acceleration, angular rate, speed, and steering sensors. A bicycle state estimator was designed to obtain additional information from this data including heading, turn rate, lean angle, steer rate, and positions of the wheels during a trajectory. The first part of the thesis describes the model setup for system identification including the Steer-to-Lean dynamics and Lean-to-Steer dynamics reduced models. CIFER software was used in the system identification process of these models. The second part describes the validation of the Empirical model by using the Rider Control model ([1]) and the Complete Rider/Vehicle model ([1]) to determine the feedback gains. The Theoretical model feedback gains were also determined by using the Rider Control model ([1]) and the Complete Rider/Vehicle model ([1]).

Contents

List of Tables

List of Figures

List of Abbreviations and Acronyms

CIFER	Comprehensive Identification from Frequency Responses software package [4]
COMPOSITE	CIFER program that combines multiple spectral windows to achieve a final frequency response [4]
DERIVID	CIFER program used to identify a state-space model structure that best fits the MIMO frequency-response database [4]
FRESPID	CIFER program that calculates SISO frequency responses using a chirp z-transform (an advanced FFT) [4]
NAVFIT	CIFER program used to identify a pole-zero transfer-function model [4]
VERIFY	CIFER program (state-space model verification) used to check the time-domain predictive accuracy of an identified model [4]
FFT	Fast Fourier transform [4]
SISO	Single-input/single-output
MIMO	Multi-input/multi-output
UART	Universal Asynchronous Receiver/Transmitter
ARM	ARM Holdings Processors Company
MEMS	Micro-electromechanical Systems
μC	Micro-controller
I^2C	Inter-integrated Circuit
LQR	Linear Quadratic Regulation
ARE	Algebraic Riccati Equation

List of Symbols

w	wheel base, m
c	trail, m
r_F, r_R	front and rear wheel radius, m
g	gravity, m/s^2
m_{rid}	mass of rider, kg
m_{bike}	mass of bicycle, kg
m_T	total mass of bicycle and rider, kg
x_T	center of mass of the total bicycle and rider, kg
λ	steer axis tilt, rad
w_x, w_y, w_z	x, y, z angular velocities, deg/s
a_x, a_y, a_z	x, y, z linear accelerations, m/s
v_f, v_r	front and rear wheel velocities, m/s
ϕ	lean angle, deg
δ	steer angle, deg
$\dot{\phi}$	lean rate, deg/s
$\dot{\delta}$	steer rate, deg/s
Ψ	heading angle, deg
$\dot{\Psi}$	turn rate, deg/s
y	lateral deviation, m
T_ϕ	leaning torque, N-m
T_δ	steering torque, N-m
p	roll angle, deg
γ^2_{xy}	coherence, (unit-less)
τ	time delay, s
ρ	phase shift, deg

Chapter 1

Introduction

1.1 A Brief Historical Review of the Bicycle

The bicycle has been an astonishing object that has propelled human-powered transportation over the last few centuries. The term *velocipede* was the common word for a human-powered vehicle with two or more wheels until the early 1870s [2]. The Karl von Drais' velocipede (1.1), that was designed as a kick-propelled two-wheeled contraption, was introduced in 1818. Other types of velocipedes included three, four, and five-wheeled machines. Other words pertaining to the number of wheels for the human-powered vehicle became more useful. Thus the trend of naming such vehicles was born. At first the bicycle was made from a wooden base that included the two wheels, a small tilter device, and short saddle. The tricycle was rider powered by using two paddles at the front wheels to propel it forward and had a pair of lateral levers that were connected to the rear wheels to incorporate steering. Other velocipedes included the unicycle and quadricycle. These were either single or multiple person vehicles.

The *original* bicycle was developed in 1867. It had been dismissed by velocipede designers due to its compact two-wheeled design since the acceptable form of transportation had more wheels. This new design began the "Boneshakers Era", which included a simple mechanical crank that brought modern developments to the bicycle. In it's simplest form, this pedal-powered bicycle could sustain speeds of up to eight miles an hour [2]. The overall design of the bicycle changed during the 1860s, in which the horizontal frame

of the *original* bicycle became a diagonal-frame to aid in the stability of the vehicle. The material for the bicycle also changed from using a basic wooden design to cast iron.

The *Ordinary Bicycle* (1.1), debuted in the "High Wheel Era", which was developed by James Moore in 1870. It had a large wheel in the front that was forty-eight inches in diameter; this was about twice the size of the rear wheel [2]. Several safety concerns were connected to this high wheel bicycle.

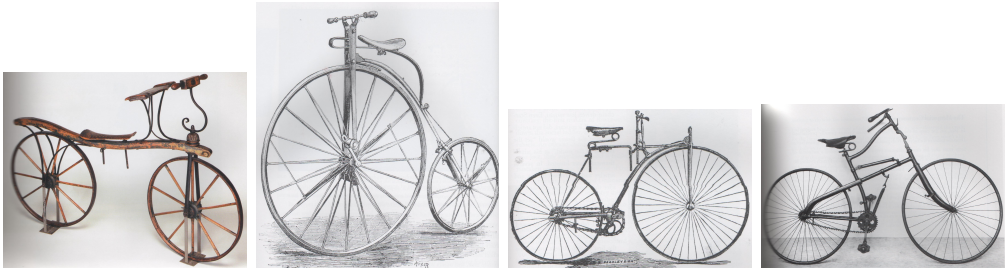

(a) (b) (c) (d)

Figure 1.1: a) Human powered *velocipede* b) *Ordinary Bicycle* c) *Rover* Safety Bicycle d) *Whippet* Bicycle. All photos are referenced from [2].

The "Safety Era" began around the mid 1880s. In 1885, the *Rover* (1.1) made its debut as a 'safer' bicycle due to its thirty-six inch diameter front wheel and thirty inch diameter rear wheel. Stanley Show displayed this "safety bicycle" that included a low-mounted frame composed of curved tubes, chains, pedals, a steering column, and sprockets [2]. Next the *Whippet* bicycle (1.1) was designed with various amounts of springs to help absorb the road shock that the smaller wheels had against the surface of the ground. It also helped to keep the body in a stationary position relative to the handlebars and pedals in the main frame [2]. Later in 1890, Show introduced pneumatic tires to the *Rover* and various bicycles after that. This increased the speed of the bicycle, and in turn it improved the overall safety of the vehicle. In addition to the pneumatic tires, the "safety bicycle" had a tilted steer axis and bent fork (like most modern bicycles) [3]. This increased the overall control and stability of the bicycle.

There had been many contributions to the study of bicycle safety and stability in the 1800s. In 1869, William Rankine qualitatively observed the steer and lean mechanics on a *velocipede*. This was the beginning of what necessary actions the rider must take to obtain self-stabilization of the bicycle. Thus, the term 'counter-steering' was introduced due to when turning one way generated a lean angle in order to keep the bicycle self-stable during a turn [5]. In 1897, Emmanuel Carvallo and Francis Whipple developed the theory behind Rankine's observations by using the rigid body dynamics equations of the "safety bicycle". They used the rigid body dynamics equations to show that at certain speeds the bicycle could become self-stable [3].

1.2 Prior Bicycle Modeling Efforts

The dynamics and stability of bicycles have been studied lately with the involvement of a human rider. The linearized bicycle model (equation 3.1) describes the lean and steer equations with respect to the inputs (T_ϕ and T_δ). This equation was implemented in the feedback models of the Bicycle Rider Control model and the Complete Rider/Vehicle model [1]. The Bicycle Rider Control model was structured for a roll control, which includes T_δ as an input. These feedback models show how the sensory information of the human can be connected to the dynamics of the bicycle. The proprioceptive, vestibular, and visual systems are included with reference to the neuromuscular model to show how the rider determines δ, ϕ, and $\dot{\phi}$ during a maneuver. The Complete Rider/Vehicle model augments the visual system with respect to how the rider and vehicle are connected to complete the maneuver in terms of Ψ and y. In addition, ϕ, δ, $\dot{\phi}$, $\dot{\delta}$, Ψ, and y results that are extracted from these models help understand the rider's control strategy for the experiment.

1.3 Team Contribution

The Brompton bicycle project overall was a team effort where several people contributed their time and knowledge to this project for two years. The participants of this team included Andrew Feit, Simon Shuster, Vishnuu Mallik, Katie Heinemann, Topher Sikorra, Maninder Grover, and myself. The team's members and instrumentation of the

bicycle varied from year to year. During this first year, the Brompton Bicycle involved sensors that would transmit the data through a Wi-Fi connection and was embedded in ROS (Robotic Operating System) code. Vishnuu Mallik contributed his time to work on these sensors and incorporated Arduino code into the ROS program. He also was the original rider/driver for the bicycle. Topher Sikorra contributed to this project in the early months by building the velocity sensors to both wheels. Maninder Grover contributed to this project with building Solidworks models for the front basket (to hold various sensors), saddle, and the handlebars. Grover also contributed to the early work for the MATLAB simulations of the bicycle. Katie Heinemann provided human modeled graphics that displayed a visual connection from Hess' feedback loops to the human body.

Andrew Feit contributed to modeling the bicycle in several MATLAB simulations including building the bicycle state estimators that involved Kalman and Extended Kalman filters to estimate the unknown parameters. Feit also contributed his knowledge of bicycle dynamics, various aspects of control theory, and aided in the development of underlying codes for several of the sensors on the bicycle. Simon Shuster incorporated new instrumentation including an ARM mini PC (to collect the data from the sensors), built newer versions of the velocity sensors, and built the steering sensor to the bicycle. Shuster updated the SolidWorks software model of the bicycle to represent the actual real bicycle by changing various properties and materials. He also include the sensors and a human rider (to model his body) to the Solidworks software model. Shuster also assisted in running experiments (as the rider in some cases). In addition, Shuster also contributed in modeling the bicycle in MATLAB simulations with developing complimentary filters for some of the unknown parameters, transfer function development, and Simulink modeling.

My contributions to this project was spread out in several stages over the past two years. In the beginning, I helped by adjusting different aspects to the older Solidworks software model of the bicycle by adding a weight to represent the human rider. I contributed to several MATLAB codes especially with respect to the state-space model simulations, bicycle control feedback loops ([1]), and analyzed data from the bicycle

state estimator that included the new instrumentation. Feit and Shuster assisted in the analysis of the reduced models for the implementation into the CIFER software. They both shared many techniques with running the experiments, extracting the data, and using the software. I used these techniques to analyzed the data that was implemented into and extracted from the CIFER software.

1.4 Motivation and Goals

The main motivation for this project is to understand how a human rides a bicycle. In general, a human uses their whole body to control and stabilize bicycle during a manuever. The humans' arms control the handlebars for steering the bicycle. The humans' legs provide power to the pedals and aids in stabilizing the bicycle during turns. The humans' visual system provides perception. The humans' ears provide a sense of balance and spatial orientation during a maneuver. Lastly, the humans' brain ties the whole body together by giving directions to each of these parts in order to safely control and stabilize the bicycle during a manuever. The Brompton bicycle was used to gain a better understanding of this motivation.

The modeling aspects of the Brompton bicycle were used in the system identification process for determining the reduced order models. The reduced order models were used to determine the lean and steer dynamics of the bicycle. These models can be explained with two different physical meanings including balancing an inverted pendulum on a moving cart and a rolling coin. The Steer-to-Lean reduced model can be thought of as balancing an inverted pendulum on a moving cart since we want to identify the bicycle's lean dynamics only. The Steer-to-Lean experiments involved a rigid rider on the bicycle, which did not allow any application of leaning torque. The Lean-to-Steer reduced model can be thought of as a rolling coin, since we want to identify the bicycle's steer dynamics only. The Lean-to-Steer experiments did not involve a rider on the bicycle. Instead it was pushed from behind allowing the steering column to freely oscillate. These experiments did not allow any steering torque to be applied to the bicycle. Therefore, reduced models did not involve external torques measurements from the bicycle. The Steer-to-Lean reduced model involved an input of steer rate ($\dot{\delta}$). The

Lean-to-Steer reduced model involved an input of lean rate ($\dot{\phi}$). The model setup for system identification section describes these reduced order models in further details.

The bicycle can be used as a platform for path planning and for analyzing human guidance behavior in a variety of situations. Some of these situations include determining the safest route for the rider in highly congested traffic areas. The motivation of using a first person perspective platform provides ample opportunities to see how guidance and perception are determined during a given trajectory. Understanding the human sensory information (visual, proprioceptive; vestibular) systems that are connected to the control of the bicycle in an attempt to avoid the obstacle on a set trajectory path is important. Other essential motivations for this work include biker's situational awareness, attention, overall vehicle dynamics, and handling qualities. Human and bicycle factors have to be considered within these situations. Some of the human factors to consider includes handling characteristics, positional aspects, and aptitude for the type of bicycle. Some of the bicycle factors include the mass properties, geometry of the tires, overall dynamics, and maneuverability.

The goals of this project can be split into two levels. The lower level goals include creating the instrumentation on the bicycle, the bicycle state estimator, and increasing the accuracy of the dynamic model. The higher level goal includes the overall system identification of the bicycle. Another higher level goal is to compare the results of the Empirical model and the Theoretical model when inputted into the Complete Rider/Vehicle model (6.1 [1]).

1.5 Overview of Our Work

The Brompton bicycle was used as an experimental platform to model the human rider in a dynamic control system. Various sensors on the bicycle provided information for the dynamic model in the form of measurements to perform system identification modeling. The data from these sensors provided information on steer angle (δ), velocity, 3-axes acceleration, and 3-axes angular velocities of the bicycle during a given trajectory. The bicycle state estimator was used to obtain additional information from this

data including heading (Ψ), turn rate ($\dot{\Psi}$), lean angle (ϕ), steer rate ($\dot{\delta}$), and positions of the wheels during a trajectory. The Brompton Bicycle Platform section describes the software and hardware used for these sensors in more detail. Various types of experiments were conducted including Steer-to-Lean dynamics, Lean-to-Steer dynamics, and lane change maneuvers. The model setup for system identification of the bicycle used Steer-to-Lean and Lean-to-Steer dynamics experiments to highlight the varying frequencies for each type. The system identification section describes this process with several packages in the CIFER software. The Empirical model was validated by using the Rider Control model ([1]) and the Complete Rider/Vehicle model ([1]) to determine the feedback gains. In addition, a comparison of the Empirical model to the Theoretical model was obtained for these feedback gains.

The following structure outlines the flow of this thesis. In Chapter 2, the Brompton Bicycle Platform is described in detail this includes the physical characteristics, instrumentation, and the bicycle state estimator. Chapter 3 provides details about the linear bicycle model equation, where it originates from, and the formation of the state space model equation. This chapter also introduces the model setup for system identification which describes in details the reduced order model systems that were used in the system identification process using CIFER in chapter 5. Chapter 4 shows the Data Collection Experiments that were used for various stages in the system identification of the Brompton bicycle. Chapter 5 describes several details of the system identification process with using CIFER software. This chapter also contains the results of system identification process using CIFER software including the frequency response method, identification of the state-space model derivatives, and the time domain verification. Lastly, it also describes the setup of the Empirical model based on the details of the model setup for system identification and the identified state-space model derivatives. Chapter 6 describes the Bicycle Rider Control model, the Complete Rider/Vehicle model, and the neuromuscular model ([1]) in detail. This chapter describes the implementation of the Empirical and Theoretical models into the Complete Rider/Vehicle model. In addition, this chapter defines the Linear Quadratic Regulation method, observable, and controllable models. Determining the feedback gains from the Complete Rider/Vehicle model is outlined with the Linear Quadratic Regulation method and the nested loops of this

model is further discussed. In addition, the results for the gains are determined and the validated model is shown by the comparison of the simulated and actual experimental results. Chapter 7 serves as a conclusion and future goals section for this thesis. In addition, there are two appendices that include Bicycle Coefficient Equations and Additional Formulas.

Chapter 2

Brompton Bicycle Platform

This chapter describes the physical properties and instrumentation of the bicycle including sensors, processors, communication, and software. This chapter also describes the bicycle state estimator.

2.1 Physical Characteristics of the Brompton Bicycle

The Brompton bicycle is a European folding bicycle that was patented in 1976. The compact design of the 16-inch wheels and hinged-frame made it simple to fold the bicycle for easy transportation and storage. There are several model types, which include different shaped handlebars, gear choices, fixtures, and material options. Most of the models consist of a steel main tube and stem. The handlebars and other components of the bicycle are made from aluminum. The rear triangle and the fork consist of titanium.

(a) (b)

Figure 2.1: Brompton Bicycle pictures a) with M-shaped handlebars b) Folded version with upright handlebars.

The rear triangle is pivoted that allows the bicycle chain to stay within the same alignment when being folded. The slight arch in the main frame allows the bicycle's front wheel to swing around from the parked position. The final folded bike dimensions are 585mm high x 545mm long x 270mm wide. The total weight of the bicycle weighs between 20-28 lbs depending on the configuration. The physical properties of the bicycle include the front wheel (F), rear wheel (R), handlebars (H), rear body frame (B), trail (c), wheel base (w), and steer-axis tilt (λ). The Brompton bicycle was compared to the Whipple bicycle model (3) when determining the mass moments of inertia and properties.

(a) (b)

Figure 2.2: a) Brompton Bicycle with real human rider b) Solidworks model of the Brompton Bicycle and the rider.

The Solidworks model of the human rider was modeled after one of the team participants. It was important to model the rider in Solidworks to be as similar to a real human rider since actual dimensions were used. In addition, this team participant was the rider for the Steer-to-Lean dynamics experiments. The real dimensions of the rider's arms, limbs, and mass was used in the Solidworks creation. This helped gain a better understanding to the exact location of where the center of mass of the rear frame of the bike and the human rider existed.

Property	Symbol	Value	Units
Wheel base	w	1.06	m
Trail	c	0.03	m
Wheel radius	$r_F = r_R$	0.21	m
Mass of the Rider	m_{rid}	59.0	kg
Mass of the Bicycle	m_{bike}	11.2	kg
Total Mass	m_T	70.2	kg
Steer Axis Tilt	λ	0.297	rad

Table 2.1: Physical Properties of the Solidworks model of the Brompton Bicycle and the rider.

2.2 Instrumentation

This section describes the Brompton bicycle platform with the Instrumentation.

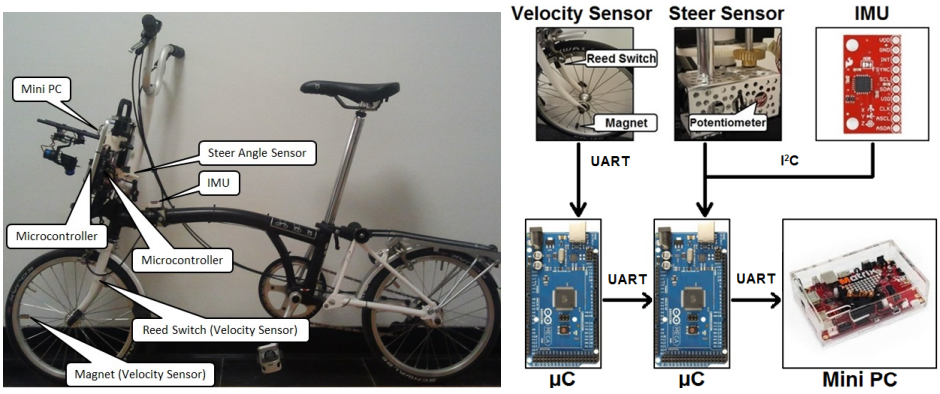

(a) (b)

Figure 2.3: Brompton Bicycle a) Full bicycle platform with labeled sensors b) block diagram of the sensors.

The front and rear pictures of the basket shows a detailed placement of the instrumentation on the Brompton bicycle.

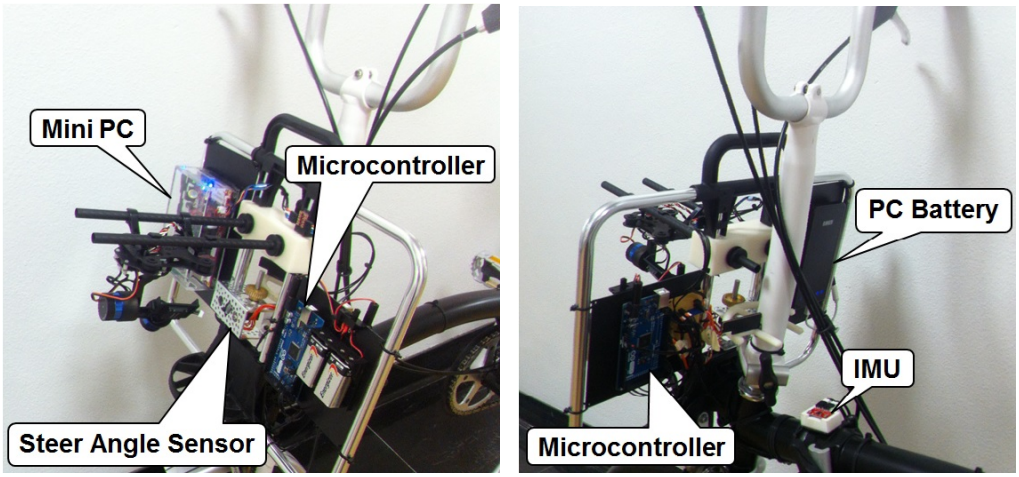

(a) (b)

Figure 2.4: Brompton Bicycle Instrumentation of the basket a) Front view b) Rear view.

The details of the instrumentation that was used on the bicycle is described below.

Inertial Sensor Inertial Measurement Unit (IMU) data is measured using the MPU-6050, which is a MEMS-based device that combines a 3-axis gyroscope and 3-axis accelerometer. The sensor transmits linear accelerations and angular velocity rates over an I^2C bus. It is mounted on a horizontal section of the bike frame near its center of mass. Offsets were calculated before each test run to calibrate the IMU.

Velocity Sensors Reed switches are mounted on the front and rear forks. As the wheels turned, magnets attached to the spokes passed by the switches and briefly closed them. The resulting high voltage pulses indicate the revolutions of each wheel.

Steer Sensor A contraption was designed to measure the steer angle of the bike. An IC Encoder was attached to the pinion gear to measure rotation. A larger gear with the same pitch was 3D printed and attached to the handlebar rod of the bike such that it was in contact with the pinion gear. This encoder was connected to the Arduino and with the aid of a separate algorithm the output measured the precise steer angle.

Processors Two Atmega2560-based Arduino Mega micro-controllers are used to receive and process data from each measurement device. One C reliably reads high pulses from the reed switches by incorporating hardware interrupts and software de-bouncing. It calculates the velocity of each wheel from their revolution rates. This data is transmitted over UART to a central C. It receives serial data indicating velocity, IMU data over I^2C, and raw voltages from the potentiometer, which are converted to a valid steer angle.

Communication and Software The central C transmits data over UART at 50 Hz to an ARM mini PC running *Ubuntu Operating System*. The mini PC executes a python program on boot that logs data into a text file. The python program creates

new text files every time there is a pause in the received serial data. This occurs when a switch controlling the power supply to the Cs is turned off. Each time a test run is to be recorded, the switch is turned on and data is logged into a new text file that is stored in a directory on the mini PC. This system allows experiments to be run in any environment or location without the need for Wi-Fi or computer receiving telemetry.

2.3 Bicycle State Estimator

A state estimator was developed for the analyzing the data extracted from the instrumentation on the bicycle. Lean angle (ϕ) was determine with a complimentary filter that multiplied a stabilization factor to the original lean angle, the angular velocity of x, and the roll angle (p). The complimentary filter was used to correct the drift in values when integrating w_x.

$$\phi = 0.99(\phi + w_x) \ + \ 0.01(p) \tag{2.1}$$

The turn rate ($\dot{\Psi}$) is determined by including the Lean Angle from the complimentary filter equation (2.1).

$$\dot{\Psi} \ = \ w_y sin(\phi) + w_z cos(\phi) \tag{2.2}$$

Heading is determined from integrating the turn rate and then multiplying by the time step (dt).

$$\Psi \ = \ \int (\dot{\Psi}) dt \tag{2.3}$$

In order to calculate a better looking graph for the front and rear wheel position of the bicycle a bias had to be included in the turn rate, heading, and steer angle equations. Therefore the equations with biases are shown below.

$$\dot{\Psi}_{bias} = \dot{\Psi} - \dot{\Psi}_{ave} \tag{2.4}$$

The heading equation with a bias equation is

$$\Psi_{bias} = \int (\dot{\Psi}_{bias}) dt - heading_{bias} \tag{2.5}$$

where, the $heading_{bias}$ referred to an arbitrary factor for each data set. Lastly, the steer angle equation with a bias

$$\delta_{bias} = \delta - \delta_{ave} \tag{2.6}$$

The velocity equations are determined for the front and the rear wheels of the bicycle including the biases described above. The arbitrary factor (arb_{factor}) is determined by each data set. The front wheel equations for x-axis and y-axis are determined with the steering angle.

$$\dot{x}_f = (v_f * (arb_{factor}))cos(\Psi_{bias} + \delta_{bias}) \tag{2.7}$$

$$\dot{y}_f = (v_f * (arb_{factor}))sin(\Psi_{bias} + \delta_{bias}) \tag{2.8}$$

The rear wheel equations for x-axis and y-axis are the following

$$\dot{x}_r = v_r cos(\Psi_{bias}) \tag{2.9}$$

$$\dot{y}_r = v_r sin(\Psi_{bias}) \tag{2.10}$$

Therefore the position equations for the front and rear wheels are the integrated forms of the velocity equations. The front wheel equations are shown below. The front wheel equation respect to the x-axis includes an added value of the wheel base (w).

$$x_f = \int (\dot{x}_f)dt + w \tag{2.11}$$

$$y_f = \int (\dot{y}_f)dt \tag{2.12}$$

The rear wheel equation for the x-axis and y-axis are

$$x_r = \int (\dot{x}_r)dt \tag{2.13}$$

$$y_r = \int (\dot{y}_r)dt \tag{2.14}$$

Chapter 3

Bicycle Model

Meijaard determined the non-linear and linearized equations of motion for the Whipple bicycle model (3.1). He provided the generalized equations of motion, the determination of the mass moments of inertia, and properties for the Whipple bicycle. His equations for determining the mass moments of inertia and how the properties of the bicycle are defined are shown in the Appendix A. The Whipple bicycle model also shows a visual description of layout of these properties (3). His work has been referenced here for determining how the Brompton bicycle is modeled in the same format.

By using the similar format as Meijaard's Whipple bicycle model the linear model for the Brompton bicycle can also be setup based on the moments of inertia and mass properties. The mass moments of inertia and properties were generated from the Solidworks model (figure 2.1). The Brompton bicycle was also modeled to include a rider. The Solidworks model of the rider included actual dimension of a real human. The Solidworks modeling was completed by Simon Shuster, in which he modeled his own body for the rider's dimensions. Side by side pictures of the real human rider on the actual Brompton bicycle and the Solidworks model is shown 2.1 and 2.1. The bicycle was separated into four sections as shown in (figure 3). The four sections include the Body, Front frame, Rear wheel, and Front wheel. Dividing the bicycle into four separate sections made it easier to calculate the mass properties and moments of inertia for each reference frame.

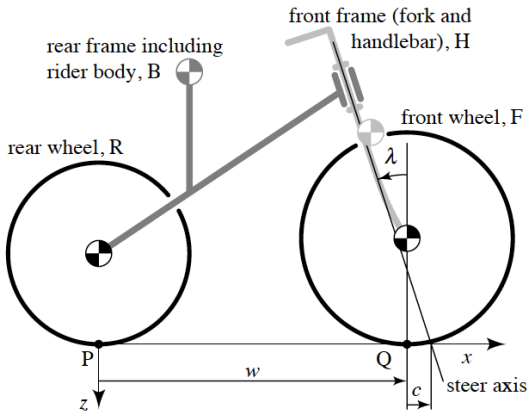

Figure 3.1: This figure shows the layout of the basic bicycle model parameters including the Body, Front frame, Rear wheel, and Front wheel [3].

This information was entered into the general equation of the linear bicycle model,

$$[M]\ddot{q} + v[C_1]\dot{q} + g([K_0] + v^2[K_2])q = [f] \tag{3.1}$$

where,

$$q = \begin{bmatrix} \phi & \delta \end{bmatrix}' \quad and \quad [f] = \begin{bmatrix} T_\phi & T_\delta \end{bmatrix}' \tag{3.2}$$

The bicycle's rear-frame ϕ is measured with respect to the vertical axis. A positive roll corresponds to a clockwise rotation when viewed from behind the frame. The steering angle δ is measured from the handlebars. It is positive for a clockwise rotation when viewed from above the frame. The external applied T_ϕ is defined about a line connecting the wheel contact points. It is positive clockwise when viewed from behind the frame. The resultant torque of all rider-applied handlebar forces is defined about the steer axis between the fork and the rider/frame it is positive clockwise when viewed from above is T_δ. The bicycle's velocity (assumed constant) is given by v. $[M]$, $[C_1]$, $[K_0]$, and $[K_2]$ are 2x2 constant matrices, which are functions of the rider and bicycle parameters given by the Solidworks software model and the equations represented in [3]. These matrices are defined further in Appendix A.

3.1 State Space Equation Form

The state space equation describes the behavior of the bicycle about a straight and upright equilibrium of constant speed v. The inputs are the steering torque (T_δ) and the leaning torque (T_ϕ). The state vector includes the lean angle (ϕ), steering angle (δ), lean rate ($\dot{\phi}$), and steering rate ($\dot{\delta}$). The layout of the state space equation is the following:

$$\dot{x} = Ax + Bu \quad (state \;\; equation) \tag{3.3}$$

$$y = Cx + Du \quad (output \;\; equation) \tag{3.4}$$

where the states and the inputs are

$$x = \begin{bmatrix} \phi & \delta & \dot{\phi} & \dot{\delta} \end{bmatrix}' \qquad u = \begin{bmatrix} T_\phi & T_\delta \end{bmatrix}' \tag{3.5}$$

Therefore the state-space equation for the bicycle is:

$$\begin{bmatrix} \dot{\phi} \\ \dot{\delta} \\ \ddot{\phi} \\ \ddot{\delta} \end{bmatrix} = \begin{bmatrix} 0_{\{2x2\}} & I_{\{2x2\}} \\ -Nn_{\{2x2\}} & -Pn_{\{2x2\}} \end{bmatrix} \begin{bmatrix} \phi \\ \delta \\ \dot{\phi} \\ \dot{\delta} \end{bmatrix} + \begin{bmatrix} 0_{\{2x2\}} \\ [M]^{-1}_{\{2x2\}} \end{bmatrix} \begin{bmatrix} T_\phi \\ T_\delta \end{bmatrix} \tag{3.6}$$

where,

$$Nn = ([M]^{-1}(g[K_0] + v^2[K_2])) \tag{3.7}$$

and

$$Pn = ([M]^{-1}(v[C_1])) \tag{3.8}$$

The output equation is written with C as a 4x4 Identity matrix and D as a 4x2 zero vector.

3.2 Model Setup for System Identification

3.2.1 Method: Frequency Response Identification

This method was used to model the bicycle's response to Steer-to-Lean and Lean-to-Steer dynamics experiments.

$$A = \begin{bmatrix} 0 & 0 & 1 & 0 \\ 0 & 0 & 0 & 1 \\ a_{31} & a_{32} & a_{33} & a_{34} \\ a_{41} & a_{42} & a_{43} & a_{44} \end{bmatrix} \begin{bmatrix} \phi \\ \delta \\ \dot{\phi} \\ \dot{\delta} \end{bmatrix} \qquad B = \begin{bmatrix} 0 & 0 \\ 0 & 0 \\ b_{31} & b_{32} \\ b_{41} & b_{42} \end{bmatrix} \begin{bmatrix} T_\phi \\ T_\delta \end{bmatrix} \tag{3.9}$$

The general approach of the system identification is designed after the bicycle linear model. The values of interest were (a_{31}, a_{32}, a_{33}, a_{34}, a_{41}, a_{42}, a_{43}, and a_{44}) of the matrix A as shown above. Also the values of interest were (b_{31}, b_{32}, b_{33}, and b_{34}) of the matrix B. The overall goal of system identification of the bicycle is to determine these unknown values.

3.2.2 Model Structure

The identification setup was based on two types of experiments. The reduced order models were determined for the Steer-to-Lean and Lean-to-Steer dynamics experiments. These modeled experiments were separated because leaning torque (T_ϕ) and steering torque (T_δ) measurements were not available on the bicycle. Therefore to determine the reduced models the variables that were directly measured (δ and $\dot{\phi}$) from the sensors on the bicycle and estimated from the bicycle state estimator (ϕ and $\dot{\delta}$) were used.

The block diagram of the Steer-to-Lean and Lean-to-Steer dynamics model (3.2) describes how the reduced models were formed. For the Steer-to-Lean dynamics model we want to identify the bicycle's lean dynamics. Thus, we use the pseudo inputs of steer angle (δ) and steer rate ($\dot{\delta}$) that are inputs into the Steer-to-Lean box in (3.2) in which we determine the a_{32} and a_{34} values. Following the connecting path to the Lean Dynamics box in (3.2) we can only provide steering torque (T_δ) as an input. This results in lean angle (ϕ) and lean rate ($\dot{\phi}$) as outputs. Similarly for the Lean-to-Steer dynamics model we want to identify the bicycle's steer dynamics. Thus, we use the pseudo inputs

of lean angle (ϕ) and lean rate ($\dot{\phi}$) that are inputs to the Lean-to-Steer box in (3.2) in which we determine the a_{41} and a_{43} values. Following the connecting path to the Steer Dynamics box in (3.2) we can only provide leaning torque (T_ϕ) as an input. This results in steer angle (δ) and steer rate ($\dot{\delta}$) as outputs. Both of these models are displayed in the equations 3.10 and 3.11 [6].

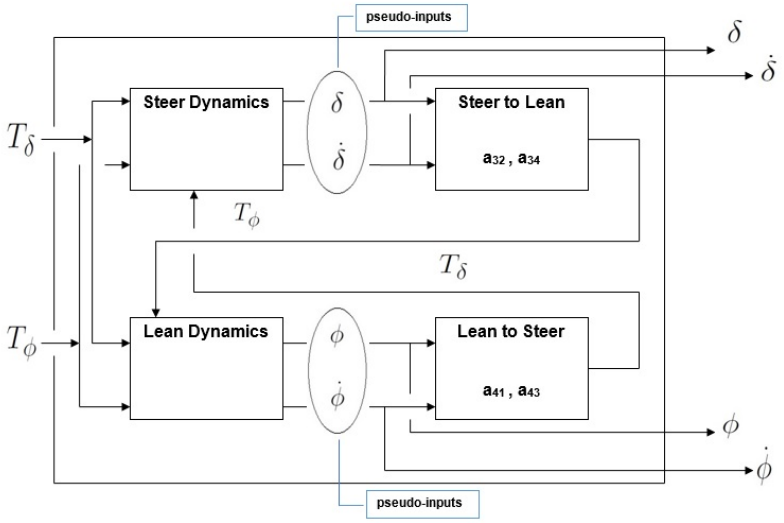

Figure 3.2: Block diagram of the Steer-to-Lean and Lean-to-Steer dynamics model.

Steer-to-Lean dynamics:

$$\begin{bmatrix} \dot{\phi} \\ \ddot{\phi} \end{bmatrix} = \begin{bmatrix} 0 & 1 \\ a_{31} & a_{33} \end{bmatrix} \begin{bmatrix} \phi \\ \dot{\phi} \end{bmatrix} + \begin{bmatrix} 0 & 0 \\ a_{32} & a_{34} \end{bmatrix} \begin{bmatrix} \delta \\ \dot{\delta} \end{bmatrix} + \begin{bmatrix} 0 & 0 \\ b_{31} & b_{32} \end{bmatrix} \begin{bmatrix} T_\phi \\ T_\delta \end{bmatrix} \tag{3.10}$$

Lean-to-Steer dynamics:

$$\begin{bmatrix} \dot{\delta} \\ \ddot{\delta} \end{bmatrix} = \begin{bmatrix} 0 & 1 \\ a_{42} & a_{44} \end{bmatrix} \begin{bmatrix} \delta \\ \dot{\delta} \end{bmatrix} + \begin{bmatrix} 0 & 0 \\ a_{41} & a_{43} \end{bmatrix} \begin{bmatrix} \phi \\ \dot{\phi} \end{bmatrix} + \begin{bmatrix} 0 & 0 \\ b_{41} & b_{42} \end{bmatrix} \begin{bmatrix} T_\phi \\ T_\delta \end{bmatrix} \tag{3.11}$$

Steer-to-Lean Model

Since in the experiments the δ and $\dot{\delta}$ are measured, this equation can be re-written to show $\dot{\delta}$ as the input. Therefore, with the implied assumption of $T_\phi = 0$ this means that the rider is rigid and only controls the bicycle by applying a steering angle. Thus, the remaining elements of the B matrix ($b_{31},\ b_{32},\ b_{33}$, and b_{34}) can be assumed very small and are left out. δ is measured by the steering sensor at the front of the bicycle by the handlebars and fork. $\dot{\delta}$ can be easily computed, by numerical differentiation. Therefore, the reduced order model can be re-written for the Steer-to-Lean dynamics as follows [6]:

$$\begin{bmatrix} \dot{\delta} \\ \dot{\phi} \\ \ddot{\phi} \end{bmatrix} = \begin{bmatrix} 0 & 0 & 0 \\ 0 & 0 & 1 \\ a_{32} & a_{31} & a_{33} \end{bmatrix} \begin{bmatrix} \delta \\ \phi \\ \dot{\phi} \end{bmatrix} + \begin{bmatrix} 1 \\ 0 \\ a_{34} \end{bmatrix} \dot{\delta} \tag{3.12}$$

Therefore the output equation is shown as,

$$\begin{bmatrix} \delta \\ \phi \\ \dot{\phi} \end{bmatrix} = \begin{bmatrix} 1 & 0 & 0 \\ 0 & 1 & 0 \\ 0 & 0 & 1 \end{bmatrix} \begin{bmatrix} \delta \\ \phi \\ \dot{\phi} \end{bmatrix} + \begin{bmatrix} 0 \\ 0 \\ 0 \end{bmatrix} \dot{\delta} \tag{3.13}$$

The ($a_{31},\ a_{32},\ a_{33},\ a_{34}$) values all contribute to the steer dynamics of the bicycle. In reference to the bicycle model ($a_{31},\ a_{32}$) refer to the top row of $([M]^{-1}(g([K_0]) + v^2[K_2]))$. Also the ($a_{33},\ a_{34}$) refers to the bicycle model top row of $([M]^{-1}(v[C_1]))$.

Steer-to-Lean Model Transfer Functions

The transfer functions from Steer-to-Lean dynamics were calculated. The $\dot{\delta}$ and $\dot{\phi}$ equations are trivial from (equation 3.12). However the following transfer functions are the most important.

$$\frac{\phi}{\dot{\delta}} = \frac{[a_{34}s + a_{32}]}{[s^3 - a_{33}s^2 - a_{31}s]} \tag{3.14}$$

$$\frac{\dot{\phi}}{\dot{\delta}} = \frac{[a_{34}s^2 + a_{32}s]}{[s^3 - a_{33}s^2 - a_{31}s]} \tag{3.15}$$

Lean-to-Steer Model

Likewise, the Lean-to-Steer dynamics model can be written in a reduced model form. This model uses $\dot{\phi}$ as an input, this is only valid when the steer torque is not applied. In this case the bicycle was essentially ridden "hands-free" with no rider involvement. The bike was pushed on the seat allowing the handlebars to move freely. T_δ and T_ϕ does not have a great influence in the $\dot{\delta}$ derivation. Therefore, the reduced model can be rewritten for the Lean-to-Steer dynamics as follows [6]:

$$\begin{bmatrix} \dot{\phi} \\ \dot{\delta} \\ \ddot{\delta} \end{bmatrix} = \begin{bmatrix} 0 & 0 & 0 \\ 0 & 0 & 1 \\ a_{41} & a_{42} & a_{44} \end{bmatrix} \begin{bmatrix} \phi \\ \delta \\ \dot{\delta} \end{bmatrix} + \begin{bmatrix} 1 \\ 0 \\ a_{43} \end{bmatrix} \dot{\phi} \tag{3.16}$$

Therefore output equation is shown with

$$\begin{bmatrix} \phi \\ \delta \\ \dot{\delta} \end{bmatrix} = \begin{bmatrix} 1 & 0 & 0 \\ 0 & 1 & 0 \\ 0 & 0 & 1 \end{bmatrix} \begin{bmatrix} \phi \\ \delta \\ \dot{\delta} \end{bmatrix} + \begin{bmatrix} 0 \\ 0 \\ 0 \end{bmatrix} \dot{\phi} \tag{3.17}$$

The ($a_{41},\ a_{42},\ a_{43},\ a_{44}$) values all contribute to the lean dynamics of the bicycle. In reference to the bicycle model ($a_{41},\ a_{42}$) refer to the bottom row of ($[M]^{-1}(g([K_0]) + v^2[K_2])$). Also the ($a_{43},\ a_{44}$) refers to the bicycle model bottom row of ($[M]^{-1}(v[C_1])$).

Lean-to-Steer Model Transfer Functions

The transfer functions from Lean-to-Steer dynamics were calculated. The $\dot{\phi}$ and $\dot{\delta}$ equations are trivial from (equation 3.16). However, the following transfer functions are the most important.

$$\frac{\delta}{\dot{\phi}} = \frac{[a_{43}s + a_{41}]}{[s^3 - a_{44}s^2 - a_{42}s]} \tag{3.18}$$

$$\frac{\dot{\delta}}{\dot{\phi}} = \frac{[a_{43}s^2 + a_{41}s]}{[s^3 - a_{44}s^2 - a_{42}s]} \tag{3.19}$$

Chapter 4

Data Collection Experiments

4.1 Experiment Setup and Procedure

A series of tests were performed to verify both the sensor data and the theoretical control model. The initial set of tests were performed in an outdoor environment. A 952 feet long and 20 feet wide bridge (Northern Pacific #9) was used for the lane change maneuvers, Steer-to-Lean Dynamics, and Lean-to-Steer Dynamics experiments. The increase in length and width aided in collection of accurate data in a single completed trial.

Figure 4.1: Northern Pacific #9 bridge located near the University of Minnesota East Bank campus.

4.1.1 Frequency Sweep Experiments

The design of the sweep experiments is important in determining the corresponding frequency responses for each reduced model. The sweeps should begin and end in trim condition. The data for trim should contain at least three seconds in the test record [4]. After the initial trim condition, two long periods inputs T_{max} should be executed. The long period inputs T_{max} correspond to the minimum frequency ω_{min}. After the long period inputs maintain a smooth increasing progression in frequency. The shorter period inputs T_{min} should be executed. This corresponds to the maximum frequency ω_{max}. The exact sinusoidal shape, constant amplitude, repeatability, and frequency progression inputs are not important in conducting the sweep experiments [4]. This is essential to ensure the coherence plot and the associated frequency response accuracy will be acceptable over the frequency range of the model [4].

Steer-to-Lean Dynamics

The following experimental data represents Steer-to-Lean low, medium, and high frequency sweeps for one trial run. This type of experiment was used to determine the frequency response of the Steer-to-Lean reduced model (equation 3.10) for system identification. In this case, the rider was rigid and only controls the bicycle by applying a steering angle.

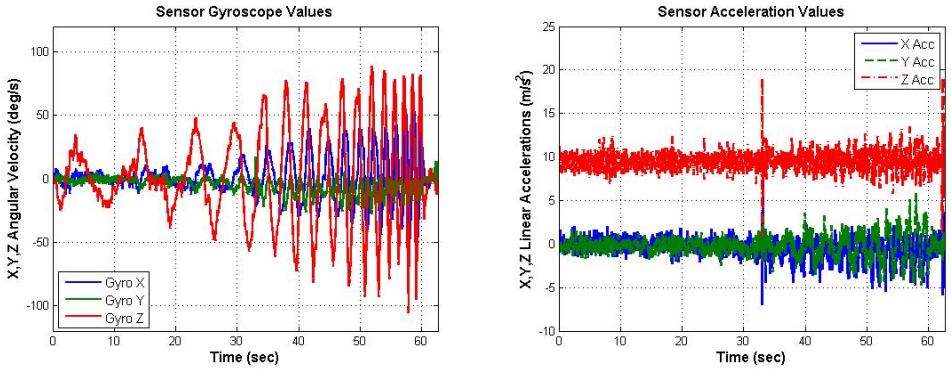

(a) (b)

Figure 4.2: Steer-to-Lean Dynamics results for a) Sensor Gyroscope values b) Sensor Acceleration values.

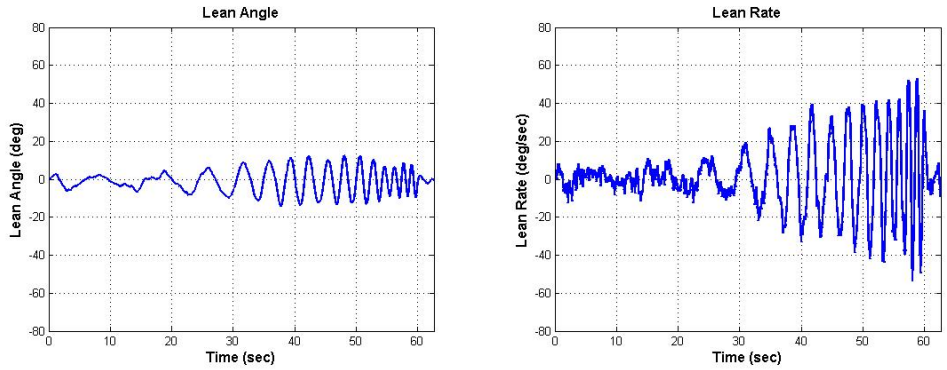

(a) (b)

Figure 4.3: Steer-to-Lean Dynamics results for a) Lean Angle b) Lean Rate.

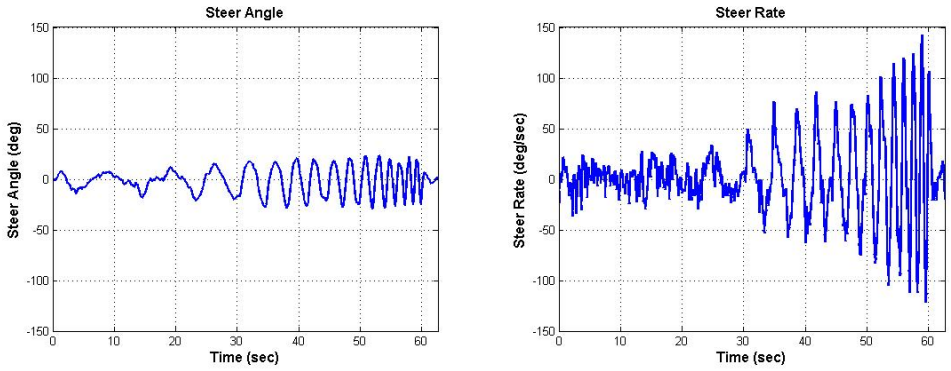

(a) (b)

Figure 4.4: Steer-to-Lean Dynamics results for a) Steer Angle b) Steer Rate.

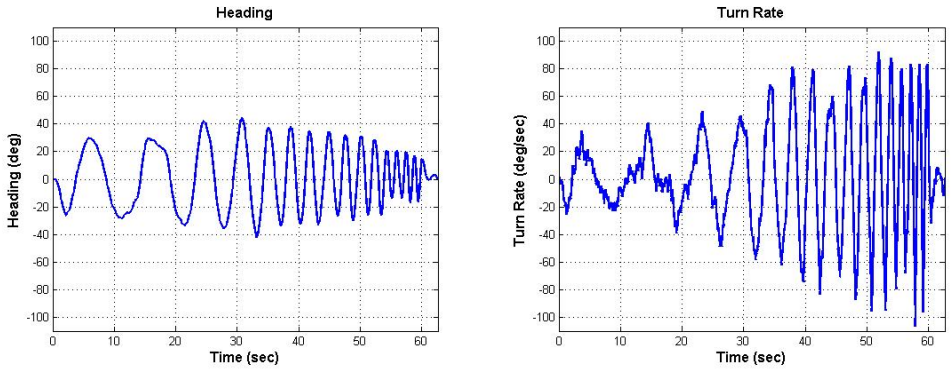

(a) (b)

Figure 4.5: Steer-to-Lean Dynamics results for a) Heading b) Turn Rate.

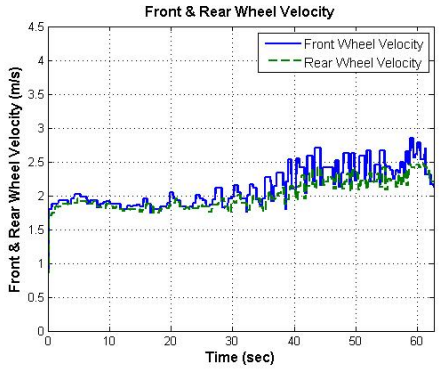

Figure 4.6: Steer-to-Lean Dynamics results for Front and Rear Wheel Velocity.

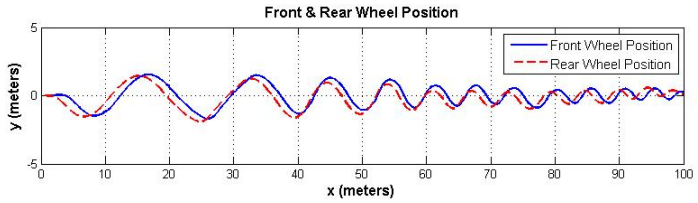

Figure 4.7: Steer-to-Lean Dynamics results for front and rear wheel position.

Lean-to-Steer Dynamics

The following experimental data represents Lean-to-Steer low, medium, and high frequency sweeps for one trial run. This type of experiment was used to determine the frequency response of the Lean-to-Steer reduced model (equation 3.11) for system identification. In this case the bicycle was essentially ridden "hands-free" with no rider involvement. The bike was pushed on the seat allowing the handlebars to move freely.

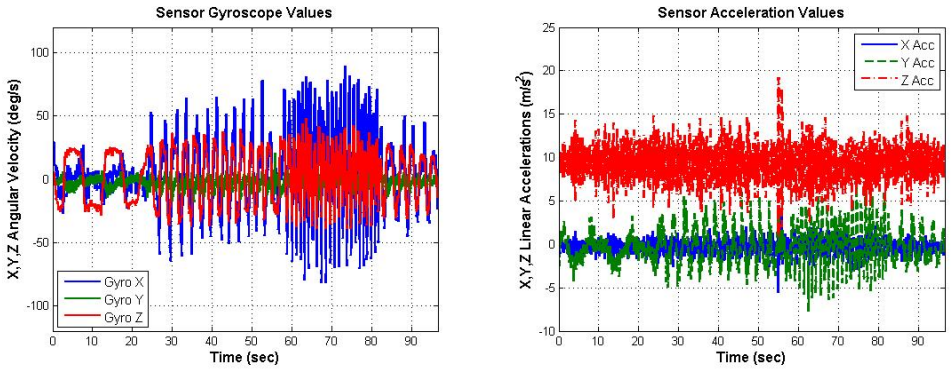

(a) (b)

Figure 4.8: Lean-to-Steer Dynamics results for a) Sensor Gyroscope values b) Sensor Acceleration values.

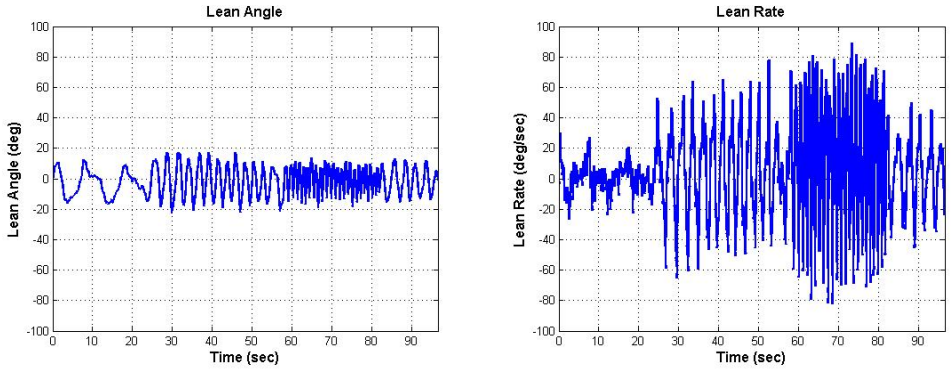

(a) (b)

Figure 4.9: Lean-to-Steer Dynamics results for a) Lean Angle b) Lean Rate.

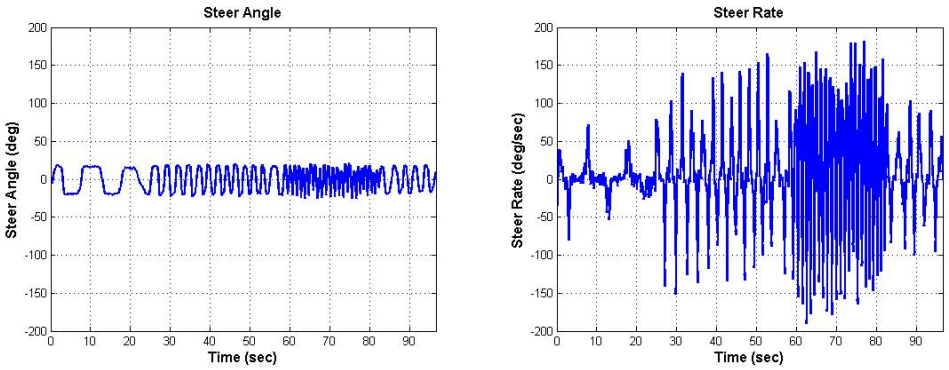

(a) (b)

Figure 4.10: Lean-to-Steer Dynamics results for a) Steer Angle b) Steer Rate.

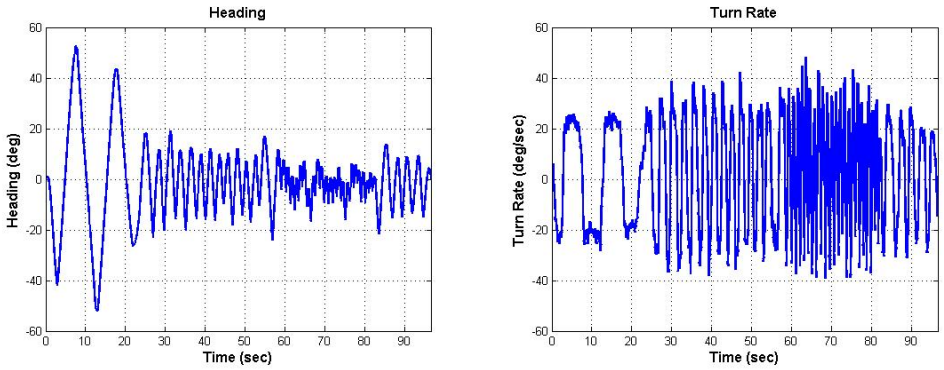

(a) (b)

Figure 4.11: Lean-to-Steer Dynamics results for a) Heading b) Turn Rate.

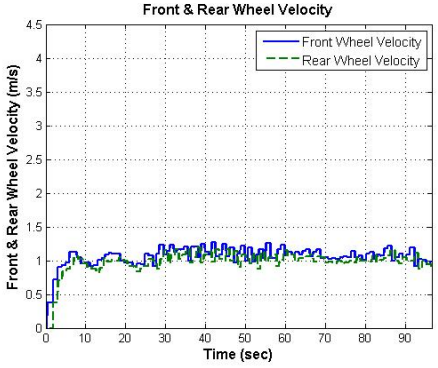

Figure 4.12: Lean-to-Steer Dynamics results for front and rear wheel velocity.

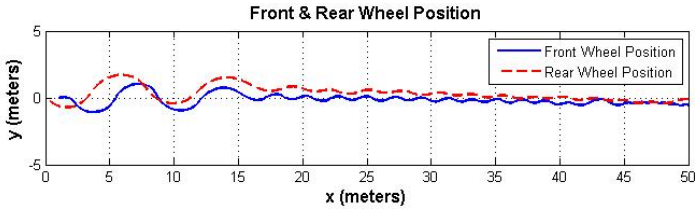

Figure 4.13: Lean-to-Steer Dynamics results for front and rear wheel position.

4.1.2 Lane Change Maneuver Experiments

Steer-to-Lean Lane Change Maneuver

As described above the Steer-to-Lean lane change maneuver also involved a rigid rider and only controls the bicycle by applying a steering angle. The following experimental data represents Steer-to-Lean Lane Change maneuver. This type of experiment was used to determine the time-domain response verification of the Steer-to-Lean reduced model (equation 3.10) for system identification.

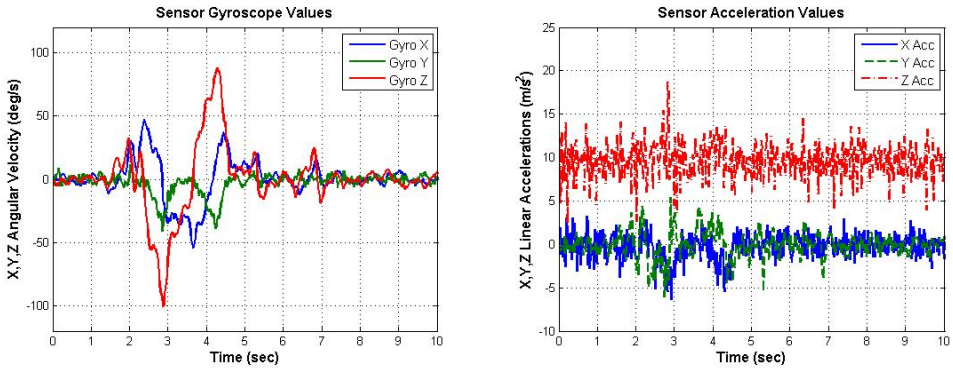

(a) (b)

Figure 4.14: Steer-to-Lean Lane Change maneuver results for a) Sensor Gyroscope values b) Sensor Acceleration values.

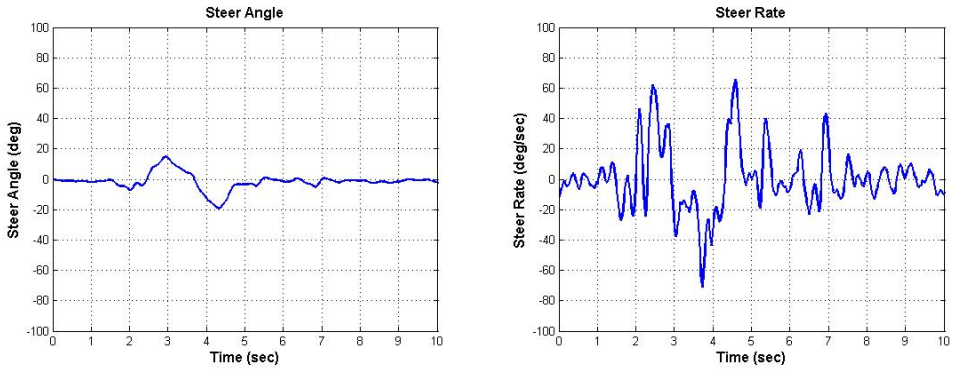

(a) (b)

Figure 4.16: Steer-to-Lean Lane Change maneuver for a) Steer Angle b) Steer Rate.

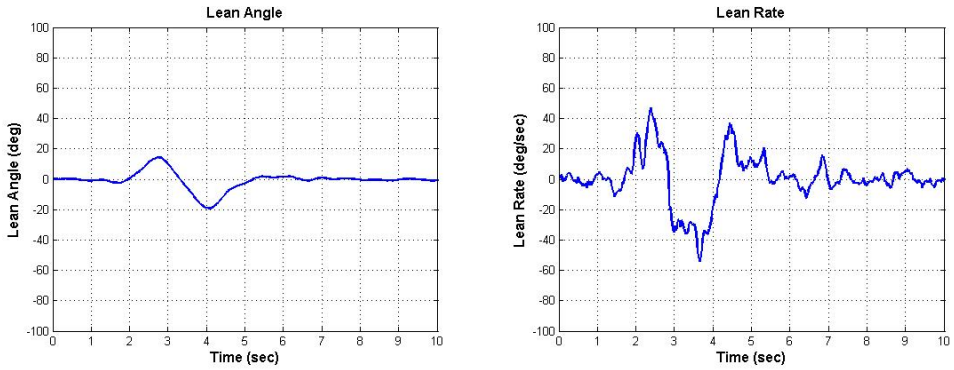

(a) (b)

Figure 4.15: Steer-to-Lean Lane Change maneuver results for a) Lean Angle b) Lean Rate.

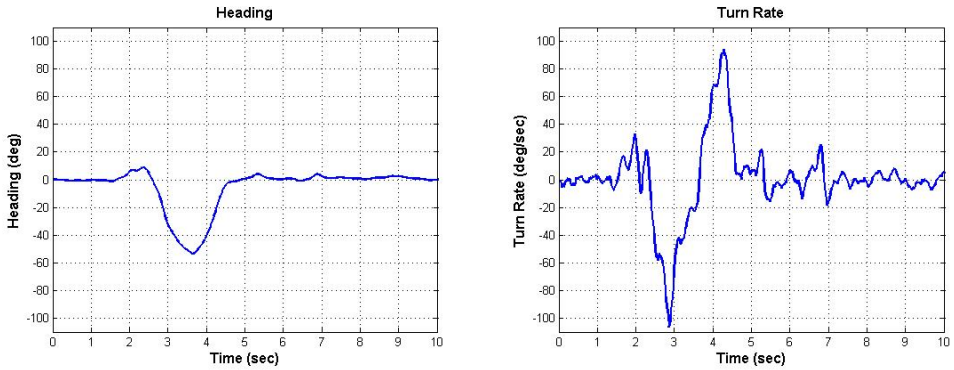

(a) (b)

Figure 4.17: Steer-to-Lean Lane Change maneuver for a) Heading b) Turn Rate.

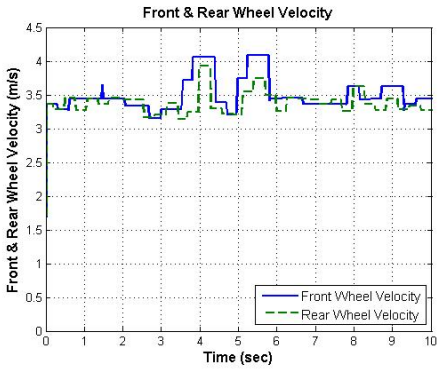

Figure 4.18: Steer-to-Lean Lane Change maneuver for front and rear wheel velocity.

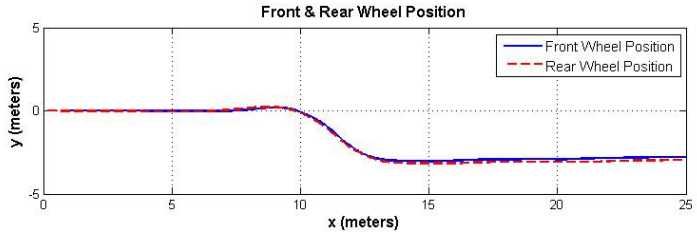

Figure 4.19: Steer-to-Lean Lane Change maneuver for front and rear wheel position.

Lean-to-Steer Lane Change Maneuver

As described above the Lean-to-Steer lane change maneuver was also ridden "hands-free" with no rider involvement on the bicycle. The bike was pushed on the seat allowing the handlebars to move freely. The following experimental data represents Lean-to-Steer Lane Change maneuver. This type of experiment was used to determine the time-domain response verification of the Lean-to-Steer reduced model (equation 3.11) for system identification.

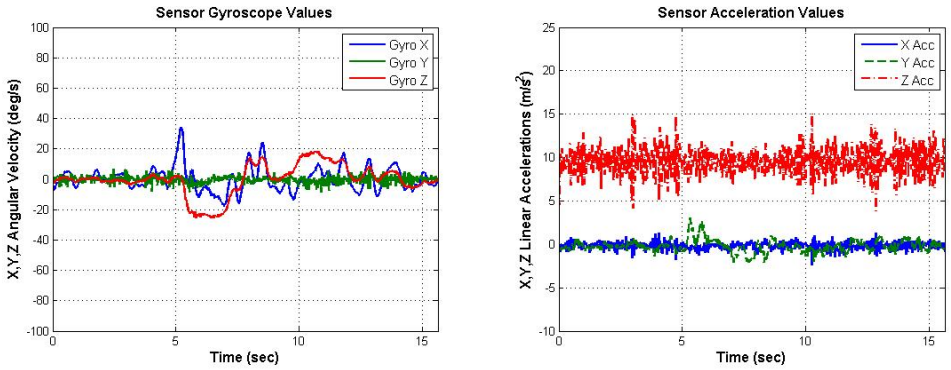

(a) (b)

Figure 4.20: Lean-to-Steer Lane Change maneuver results for a) Sensor Gyroscope values b) Sensor Acceleration values.

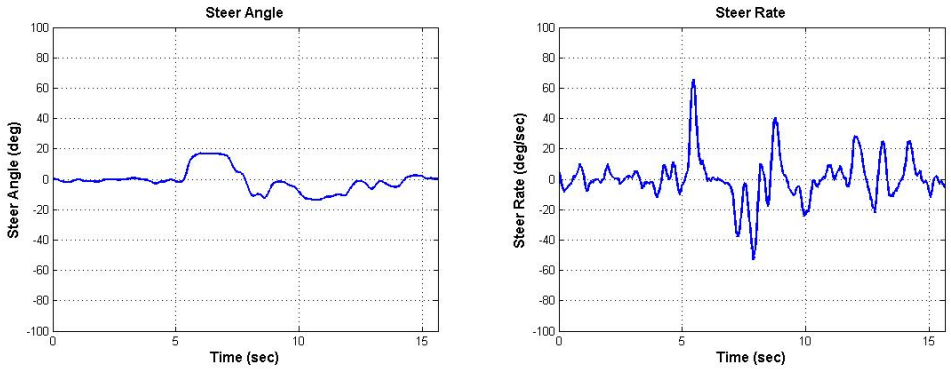

(a) (b)

Figure 4.22: Lean-to-Steer Lane Change maneuver for a) Steer Angle b) Steer Rate.

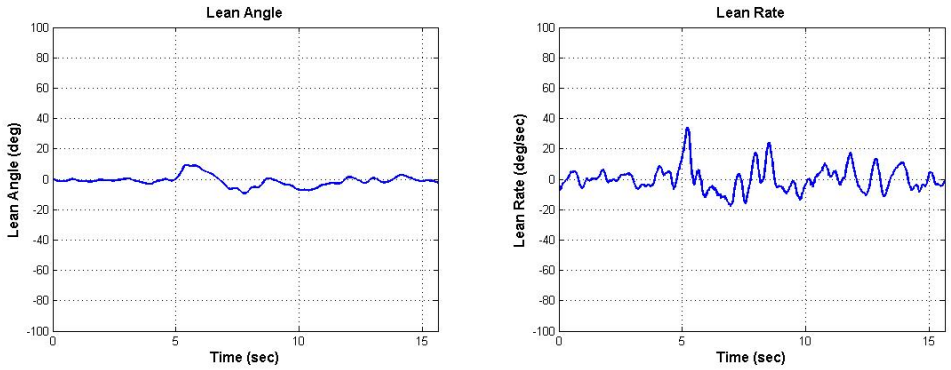

(a) (b)

Figure 4.21: Lean-to-Steer Lane Change maneuver results for a) Lean Angle b) Lean Rate.

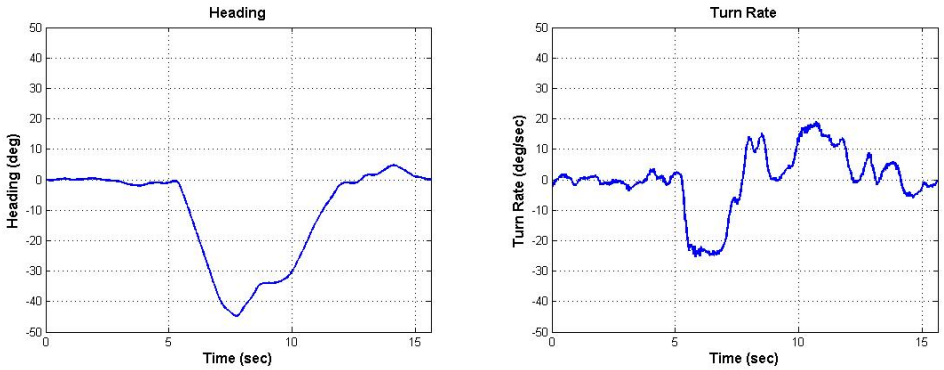

(a) (b)

Figure 4.23: Lean-to-Steer Lane Change maneuver for a) Steer Angle b) Steer Rate.

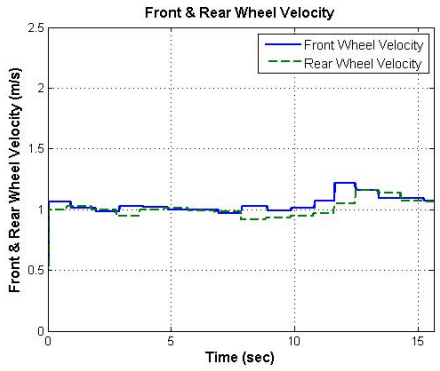

Figure 4.24: Lean-to-Steer Lane Change maneuver for front and rear wheel velocity.

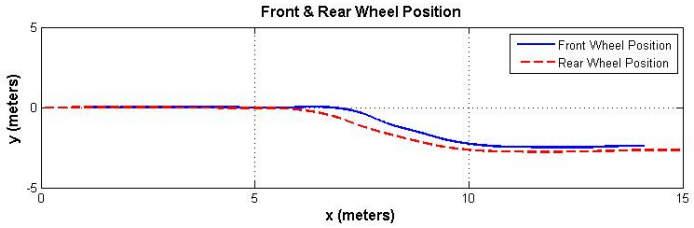

Figure 4.25: Lean-to-Steer Lane Change maneuver for front and rear wheel position.

Chapter 5

System Identification using the CIFER Software

5.1 Introduction to the CIFER Software

Several packages of the CIFER Software was used to show the system identification of the Brompton bicycle. This program was used to determine a mathematical description of the bicycle's dynamic behaviors from measured bicycle motions. The mathematical description of the bicycle's dynamic behaviors gave us insights to how the model relates to the physical understandings. The results from system identification of the Brompton bicycle will be used for simulation model validation.

The approach for identifying the bicycle's dynamic behaviors is through frequency responses analysis. The frequency response analysis was processed with the FRESPID package in the CIFER software. The Frequency Response method is used to determine the bicycle dynamics from the bicycle-test data. This method uses an unbiased *frequency-response estimate* is determined from the ratio of the input autospectrum estimate $\hat{G}_{xx}$ to the cross-spectrum estimate $\hat{G}_{xy}$ at each discrete frequency f [4]:

$$Frequency - response\ \ estimate = \hat{H}(f) = \frac{\hat{G}_{xy}(f)}{\hat{G}_{xx}(f)} \tag{5.1}$$

Thus, the choice in picking the particular spectral ratios eliminates process noise due to how the biases are chosen in the frequency response calculation. In addition, the

coherence function provides key measure of the frequency-response accuracy without any dependency of the parametric model structures [4]. The *coherence* function [4] estimate is defined as:

$$coherence = \hat{\gamma}^2_{xy}(f) = \frac{|\hat{G}_{xy}(f)|^2}{|\hat{G}_{xx}(f)||\hat{G}_{yy}(f)|} \tag{5.2}$$

Therefore our guideline for the *coherence* function [4] should satisfy the condition,

$$\gamma^2_{xy} \geq 0.6 \tag{5.3}$$

This guideline determines the accuracy of the frequency-response identification. The response identification should be within the guideline 5.3 to insure that the unreliable (noisy) data is excluded in the analysis. Therefore a frequency range will be determine where the *coherence* is best and is within the guideline.

Other important features of using a frequency-response method includes incorporating a time delay (τ) and phase shift (ρ) accuracy, elimination of biases, and reference shifts as identification parameters. In addition a frequency-response method can be used to determine the identification of systems for unstable dynamics. The identification process uses state-space model equations in the DERIVID package and similarly with transfer functions in the NAVFIT package. The state-space model equation for the state vector x to the control input u is written with respect to the time delay and a bias constant [4].

$$\dot{x} = Ax \ + \ Bu(t-\tau) \ + \ bias \tag{5.4}$$

In general, the matrix $[A]$ represents the stability derivatives, matrix $[B]$ represents the control derivatives, τ is the time delay, and a bias. The bias part of the equation includes the unknown biases. Biases are included into the equation 5.4 for unmeasurable inputs such as weather conditions, initial condition states for the inputs, biases in the assumed values for the trim-control inputs, and errors in the model structure [4]. Likewise, the output equation [4] is written as

$$y \ = \ Cx \ + \ Du(t-\tau) \ + \ y_{ref} \tag{5.5}$$

The vector of constants y_{ref} is included into the output equation to adjust the offsets in the measurement devices. The state and output equations can be rewritten into a transfer function model format.

5.2 Frequency Response Method Results using the CIFER Software

5.2.1 Obtaining Frequency Responses with the FRESPID package in the CIFER Software

Guidelines are necessary to obtain the frequency responses of your system. These include the overall design of the frequency sweep inputs, choosing the best filter bandwidth (ω_f), and sample rate (ω_s). The guideline for choosing the recommended cut-off filter bandwidth (ω_f) [4],

$$\omega_f \geq 5 * \omega_{max} \tag{5.6}$$

Once the filter bandwidth is selected the sample rate can be determined. The guideline for the sample rate (ω_s) [4],

$$\omega_s \geq 5 * \omega_f \tag{5.7}$$

The corresponding periods (T_{max} & T_{min}) can be obtained based on the minimum and maximum frequencies of interest (refer to the equations in Appendix (B)). The data record length for a single sweep should be five times the T_{max} [4]. The guideline for total sweep record length T_{rec} [4],

$$T_{rec} \geq (4\ to\ 5)T_{max} \tag{5.8}$$

5.2.2 Steer-to-Lean Dynamics

The frequency response and coherence results are shown 5.2.2, for the Steer-to-Lean Dynamics experiments. The bandwidth frequency for the full frequency range is 49.9747 Hz. The first set of results indicate the input of steer rate ($\dot{\delta}$) and output of lean angle (ϕ). Both of these results are determined from the experimental results. The frequency range for $\frac{\phi}{\dot{\delta}}$ is 0.426 $\frac{rad}{s}$ to 62.80 $\frac{rad}{s}$.

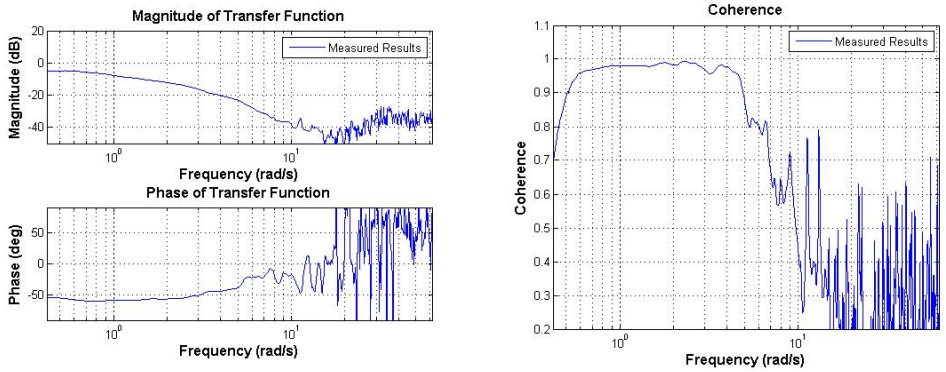

(a) (b)

Figure 5.1: Steer-to-Lean dynamics measured ($\frac{\phi}{\dot{\delta}}$) results a) Frequency Response b) Coherence.

The second set of results indicate the input of steer rate ($\dot{\delta}$) and output of lean rate ($\dot{\phi}$). The frequency range for $\frac{\dot{\phi}}{\dot{\delta}}$ is 0.426 $\frac{rad}{s}$ to 62.80 $\frac{rad}{s}$.

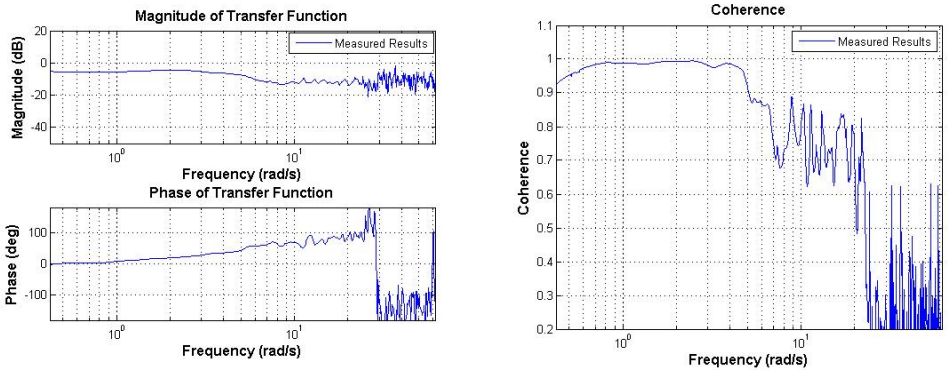

(a) (b)

Figure 5.2: Steer-to-Lean dynamics measured ($\frac{\dot{\phi}}{\dot{\delta}}$) results a) Frequency Response b) Coherence.

5.2.3 Lean-to-Steer Dynamics

The frequency response and coherence results are shown 5.2.3, for the Lean-to-Steer Dynamics experiments. The bandwidth frequency for the full frequency range is 49.338

Hz. The first set of results indicate the input of lean rate ($\dot{\phi}$) and output of steer angle (δ). Both of these results are determined from the experimental results. The frequency range for $\frac{\delta}{\dot{\phi}}$ is 0.302 $\frac{rad}{s}$ to 62.80 $\frac{rad}{s}$.

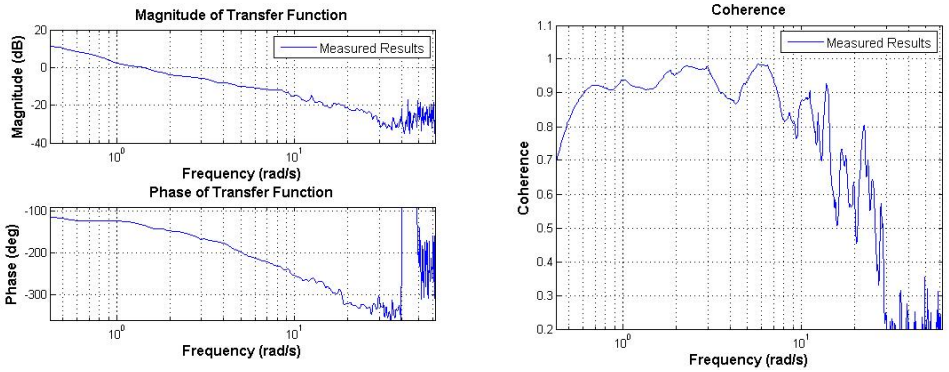

(a) (b)

Figure 5.3: Lean-to-Steer dynamics measured ($\frac{\delta}{\dot{\phi}}$) results a) Frequency Response b) Coherence.

The second set of results indicate the input of lean rate ($\dot{\phi}$) and output of steer rate ($\dot{\delta}$). The frequency range for $\frac{\dot{\delta}}{\dot{\phi}}$ is 0.302 $\frac{rad}{s}$ to 62.80 $\frac{rad}{s}$.

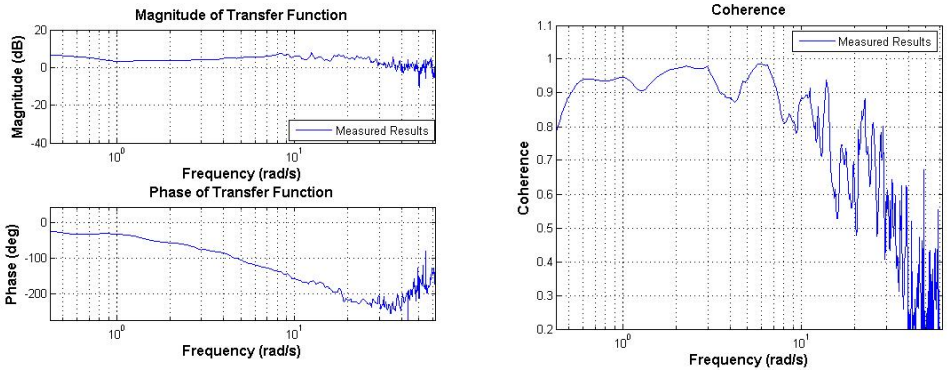

(a) (b)

Figure 5.4: Lean-to-Steer dynamics measured ($\frac{\dot{\delta}}{\dot{\phi}}$) results a) Frequency Response b) Coherence.

5.3 Identification of State-Space model derivatives using the DERIVID package in the the CIFER Software

The state-space model equations are set up as in 5.4 and 5.5 with the bicycles respective state and control inputs 3.12 for Steer-to-Lean Dynamics. The overall average cost function (J) is needed to determine the level of accuracy the model displays. Refer to Appendix (B) for further information about the overall cost function. The guideline for the overall average cost function [7],

$$J_{ave} \leq 100 \tag{5.9}$$

In addition to the overall average cost function the sensitivity values for the predicted results with respect to the measured data results are determined. These sensitivity values include Cramer-Rao bound (CR-bound), Cramer-Rao percentage (CR %), and the insensitivity percentage (INSEN %). The guidelines for each of sensitivity values are shown below.

The Cramer-Rao bounds are one of the important keys in refining the model structure for the relative values. Thus if the relative values give large Cramer-Rao bounds this indicates poor identifiability. These values should be fixed within the model structure. The Cramer-Rao bounds are best expressed as a percentage of the converged identification values [4],

$$\overline{CR_i} = \left| \frac{CR_i}{\theta_i} \right| * 100\% \tag{5.10}$$

Thus, CR_i is the ith identified parameter associated to the diagonal element of the inverse of the Hessian matrix (H)[7]. Further details on the Hessian matrix is shown in the Appendix (B). In addition σ_i describes the standard deviation obtained from many repeated maneuvers [7].

The guideline for Cramer-Rao bounds percentage [7],

$$\overline{CR_i} \leq 20\% \tag{5.11}$$

When the Cramer-Rao bounds satisfy the guideline above and the overall average cost function equation 5.9 this reflects a highly reliable state space model identification with

good predictive accuracy [7]. In addition, depending on the model structure and dynamics involved in the system large Cramer-Rao bounds may be in the range of 20%-40% without loss of reliability or cause for concern [7].

Insensitivity parameters are determined from the diagonal elements of the Hessian matrix H [4]. Thus, the insensitivity value is the lower limit of the Cramer-Rao bound. Lastly, the insensitivities values obtained from the frequency response method gives a guideline as [7]

$$\overline{I_i} < 10\% \tag{5.12}$$

In addition, depending on the model structure and dynamics involved in the system large insensitivity values are in the range of 10-20 % without loss of reliability or cause for concern.

5.3.1 Steer-to-Lean Dynamics

The extracted frequency response for the measured and predicted results are shown below. The coherence plot is also shown. The frequency range for $\frac{\phi}{\delta}$ is 0.5 $\frac{rad}{s}$ to 6.963 $\frac{rad}{s}$. The bandwidth frequency for this range is 5.541 Hz. The measured results were taken from the original frequency response and *coherence* plots in 5.2.2 section. The predicted results were determined from the identified state-space model derivatives in the DERIVID package in the CIFER Software. The goal is to identify two transfer functions (equation 3.14 and 3.15) from these state-space model derivatives.

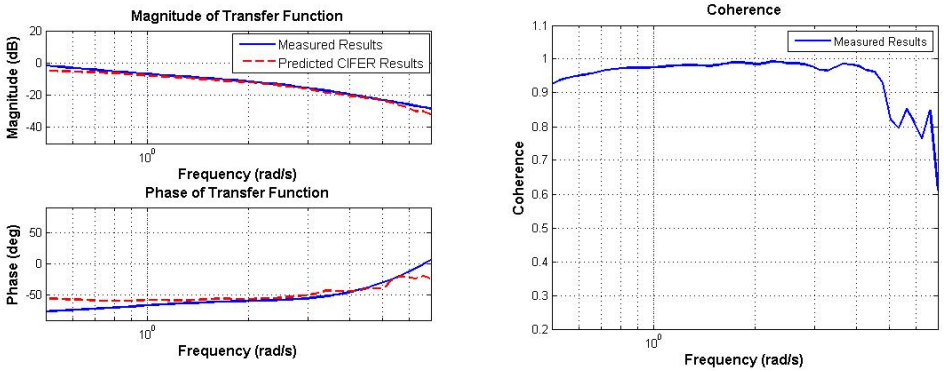

(a) (b)

Figure 5.5: Measured ($\frac{\phi}{\delta}$) and Predicted Results a) Extracted Frequency Response b) Coherence.

The measured results were taken from the original frequency response and *coherence* plots in 5.2.2 section. The frequency range for $\frac{\dot{\phi}}{\delta}$ is 0.5 $\frac{rad}{s}$ to 7.75 $\frac{rad}{s}$. The bandwidth frequency is 6.1673 Hz.

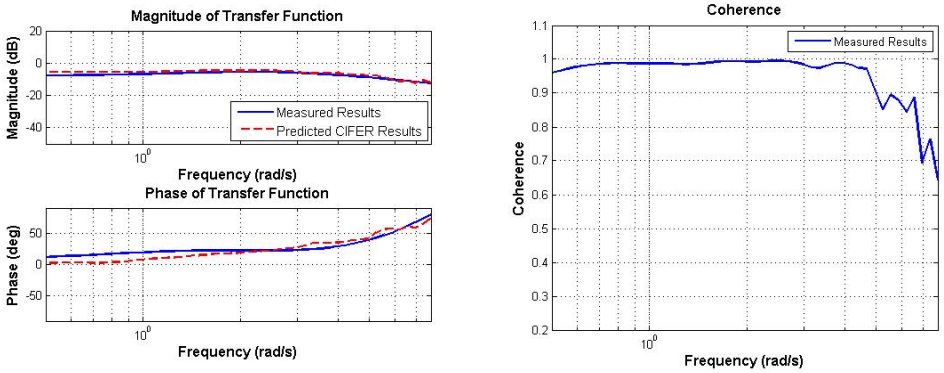

(a) (b)

Figure 5.6: Measured ($\frac{\dot{\phi}}{\delta}$) and Predicted Results a) Extracted Frequency Response b) Coherence.

Each of these predicted results had sensitivity values that were also determined by the DERIVID package. Therefore the average cost function for both of these results is 60.6997.

Parameter & Value	CR Bound	CR %	INSEN %
$a_{31} = -6.886$	1.674	24.31	1.854
$a_{32} = 2.685$	0.7872	29.31	2.157
$a_{33} = -4.118$	0.4212	10.23	1.842
$a_{34} = 1.881$	0.2282	12.13	1.802

Table 5.1: Tabulated results for Steer-to-Lean identified a_{31}, a_{32}, a_{33}, and a_{34} values with respect to Cramer-Rao bound, Cramer-Rao percent, and the insensitivity percent.

The model derivatives that were determined from DERIVID are shown above in the Steer-to-Lean reduced state-space model.

$$\begin{bmatrix} \dot{\delta} \\ \dot{\phi} \\ \ddot{\phi} \end{bmatrix} = \begin{bmatrix} 0 & 0 & 0 \\ 0 & 0 & 1 \\ 2.6855 & -6.8858 & -4.1179 \end{bmatrix} \begin{bmatrix} \delta \\ \phi \\ \dot{\phi} \end{bmatrix} + \begin{bmatrix} 1 \\ 0 \\ 1.8809 \end{bmatrix} \dot{\delta} \tag{5.13}$$

The output equation is shown as,

$$\begin{bmatrix} \delta \\ \phi \\ \dot{\phi} \end{bmatrix} = \begin{bmatrix} 1 & 0 & 0 \\ 0 & 1 & 0 \\ 0 & 0 & 1 \end{bmatrix} \begin{bmatrix} \delta \\ \phi \\ \dot{\phi} \end{bmatrix} + \begin{bmatrix} 0 \\ 0 \\ 0 \end{bmatrix} \dot{\delta} \tag{5.14}$$

From the Steer-to-Lean reduced state-space model we can find the resulting transfer functions. The first transfer function $\frac{\delta}{\dot{\delta}}$ is trivial as it is only $\frac{1}{s}$. Since the other transfer functions $\frac{\phi}{\dot{\delta}}$ and $\frac{\dot{\phi}}{\dot{\delta}}$ show the identified resulting values for a_{31}, a_{32}, a_{33}, and a_{34} these are shown with the time delays. The units for these transfer functions are $(\frac{deg}{deg})$

$$\frac{\phi}{\dot{\delta}} = \frac{1.881s + 2.686}{s^3 + 4.118s^2 + 6.886s} e^{(-0.408s)} \tag{5.15}$$

$$\frac{\dot{\phi}}{\dot{\delta}} = \frac{1.881s^2 + 2.686s}{s^3 + 4.118s^2 + 6.886s} e^{(-0.337s)} \tag{5.16}$$

5.3.2 Lean-to-Steer Dynamics

The extracted frequency response for the measured and predicted results are shown below. The coherence plot is also shown. The measured results were taken from the original frequency response and *coherence* plots in 5.2.3 section. The predicted results were determined from the identified state-space model derivatives in the DERIVID package in the CIFER software. The goal is to identify two transfer functions (equation 3.18 and 3.19) from these state-space model derivatives. The frequency range for $\frac{\delta}{\dot{\phi}}$ is 0.5 $\frac{rad}{s}$ to 7.75 $\frac{rad}{s}$. The bandwidth frequency is 6.1673 Hz.

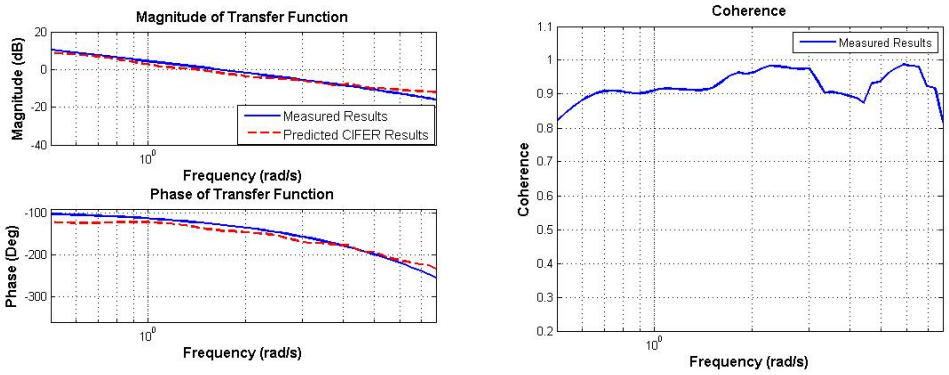

(a) (b)

Figure 5.7: Measured ($\frac{\delta}{\dot{\phi}}$) and Predicted Results a) Extracted Frequency Response b) Coherence.

The measured results were taken from the original frequency response and *coherence* plots in 5.2.3 section. The predicted results were determined from the identified state-space model derivatives in the DERIVID package in the CIFER software. The frequency range for $\frac{\dot{\delta}}{\dot{\phi}}$ is 0.5 $\frac{rad}{s}$ to 7.75 $\frac{rad}{s}$. The bandwidth frequency is 6.1673 Hz.

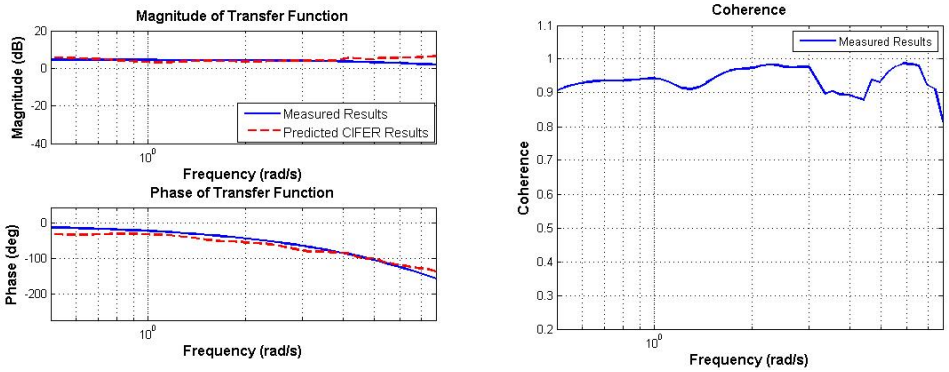

(a) (b)

Figure 5.8: Measured ($\frac{\dot{\delta}}{\phi}$) and Predicted Results a) Extracted Frequency Response b) Coherence.

Each of these predicted results had sensitivity values that were also determined by DERIVID package. Therefore the average cost function for these results is 91.0273.

Parameter & Value	CR Bound	CR %	INSEN %
$a_{41} = 0.098629$	0.2195	22.26	2.707
$a_{42} = -0.51823$	0.07991	15.42	6.786
$a_{43} = 14.314$	2.569	17.94	1.347
$a_{44} = -8.6134$	1.697	19.70	1.433

Table 5.2: Tabulated results for Lean-to-Steer identified a_{41}, a_{42}, a_{43}, and a_{44} values with respect to Cramer-Rao bound, Cramer-Rao percent, and the insensitivity percent.

The model derivatives that were determined from DERIVID are shown in 5.2 in the Lean-to-Steer reduced state-space model.

$$\begin{bmatrix} \dot{\phi} \\ \dot{\delta} \\ \ddot{\delta} \end{bmatrix} = \begin{bmatrix} 0 & 0 & 0 \\ 0 & 0 & 1 \\ 0.098629 & -0.51823 & -8.6134 \end{bmatrix} \begin{bmatrix} \phi \\ \delta \\ \dot{\delta} \end{bmatrix} + \begin{bmatrix} 1 \\ 0 \\ 14.314 \end{bmatrix} \dot{\phi} \tag{5.17}$$

The output equation is shown with

$$\begin{bmatrix} \phi \\ \delta \\ \dot{\delta} \end{bmatrix} = \begin{bmatrix} 1 & 0 & 0 \\ 0 & 1 & 0 \\ 0 & 0 & 1 \end{bmatrix} \begin{bmatrix} \phi \\ \delta \\ \dot{\delta} \end{bmatrix} + \begin{bmatrix} 0 \\ 0 \\ 0 \end{bmatrix} \dot{\phi} \tag{5.18}$$

From the Lean-to-Steer reduced state-space model we can find the resulting transfer functions. The first transfer function $\frac{\phi}{\dot{\phi}}$ is trivial as it is only $\frac{1}{s}$. Since the other transfer functions $\frac{\delta}{\dot{\phi}}$ and $\frac{\dot{\delta}}{\dot{\phi}}$ show the identified resulting values for a_{41}, a_{42}, a_{43}, and a_{44} these are shown with the time delays. The units for these transfer functions are $(\frac{deg}{deg})$.

$$\frac{\delta}{\dot{\phi}} = \frac{14.31s + 0.9863}{s^3 + 8.613s^2 + 0.5182s} e^{(-0.273s)} \tag{5.19}$$

$$\frac{\dot{\delta}}{\dot{\phi}} = \frac{14.31s^2 + 0.9863s}{s^3 + 8.613s^2 + 0.5182s} e^{(-0.259s)} \tag{5.20}$$

5.4 Time Domain Verification of the Identified Transfer Function Models

5.4.1 Overview of the Verification Process using the VERIFY package in the CIFER Software

Time-domain verification is important in determining the predictive accuracy and reliability of the identified model. Depending on how the time-domain's predictive accuracy looks respective to the guidelines listed below will determine if the frequency-response identification process might need to be repeated and adjusted. Repeating flight testings may improve the overall attention to the particular experiment to increase the noise to signal and reduced cross-control correlation [4]. In addition improving these results may lead to eliminating repeated maneuvers during the frequency sweep records that were conducted in not idealistic weather situations (ie. high wind and temperature).

The state-space model structure is written in the same form of equations 5.4 and 5.5. However, the matrices $[A]$, $[B]$, $[C]$, and $[D]$ has been replaced with the to be identified matrices. These equations are written as the following,

$$[M]\dot{x} \;=\; [F]x \;+\; [G]u(t-\tau) \tag{5.21}$$

With the output equation written as,

$$y \;=\; [H_0]x \;+\; [H_1]\dot{x} \tag{5.22}$$

The matrices $[M]$, [F], [G], and the vector τ contain model parameters to be identified in the DERIVID process. They also can contain prior model parameters and constants. The time delay (τ) is included to account for unstable dynamics in the model. The matrices $[H_0]$ and $[H_1]$ are composed of known constants in the model. The state-space model equation without including the y_{ref} and the bias terms (equation 5.4 and 5.5) can be written to accommodate the $[M]$, [F], [G], $[H_0]$, and $[H_1]$ matrices. This is written as [4],

$$[A] \;=\; [M]^{-1} \tag{5.23}$$

$$[B] \;=\; [M]^{-1} \tag{5.24}$$

$$[C] \;=\; [H_0] \;+\; [H_1][M]^{-1}[F] \tag{5.25}$$

$$[D] \;=\; [H_1][M]^{-1}[G] \tag{5.26}$$

After determining the identified parameters in the equations 5.21 and 5.22 the control input vector (u) now includes the time history data and the trim (steady-state) values. The trim values for the control input vector includes data from the initial condition of the data to be tested for the time domain verification. In addition a bias vector ($\dot{x_b}$) is included to account for the effects of noise in the 5.21 estimate of the identified parameters. Thus, the resulting equation including the bias vector becomes [4],

$$[M]\dot{x} \;=\; [F]x \;+\; [G]u(t-\tau) + \dot{x}_b \tag{5.27}$$

The bias vector is treated as a constant and does not change the dynamics of the predicted response [4]. Since a bias vector was included into the state equation (5.21) a similar reference output is needed to be included into the output equation (5.22). This is based on the time history data in the output equation (5.21). It is evaluated from subtracting out the trim (steady-state) reference output from this original data record. Thus, this creates an output estimate known as the reference-shift vector y_{ref}. Thus, the resulting equation including the reference-shift vector becomes [4],

$$y \;=\; [H_0]x \;+\; [H_1]\dot{x} \;+\; y_{ref} \tag{5.28}$$

The values for the bias and reference-shift vectors are estimated based off the solution to the weighted least-squares error function and the cost function (J). Further information about these equations are in Appendix B. In general, the guidelines for the cost function for the *rms fit error* is [4],

$$J_{rms} \leq \; 1.0 \; to \; 2.0 \tag{5.29}$$

This reflects the acceptable level of accuracy for the dynamics in modeling the error function that is calculated based on the units provided in the model (B.9).

The *Theil inequality coefficient (TIC)* equation is shown in Appendix B with equation B.11. The guideline for the *Theil inequality coefficient (TIC)* equation is [4],

$$TIC \;\leq\; 0.25 \; to \; 0.30 \tag{5.30}$$

This is based on a good predictive agreement. A model with perfect predictive capability implies a TIC value equal to zero. However, a model with no predictive capability corresponds with a TIC value equal to one.

5.4.2 Time-Domain Results

Steer-to-Lean and Lean-to-Steer lane change maneuver experiments were used to test the verification of the unknown variables (a_{31}, a_{32}, a_{33}, a_{34}, a_{41}, a_{42}, a_{43}, and a_{44}) that were determined in the DERIVID package with the state-space model structure. These experiments were completed on the 952 feet long and 20 feet wide bridge (4.1) with similar weather conditions as the respective frequency sweeps experiments. The lane change experiment occurred approximately 50 feet from the start of the bridge and it included a 14 feet lane change maneuver.

Steer-to-Lean Dynamics

The time domain verification predicted results from the DERIVID package is plotted against the measured data. The VERIFY package in the CIFER software used the input of steer rate from a lane change maneuver to establish the predicted output results for steer angle, lean angle, and lean rate.

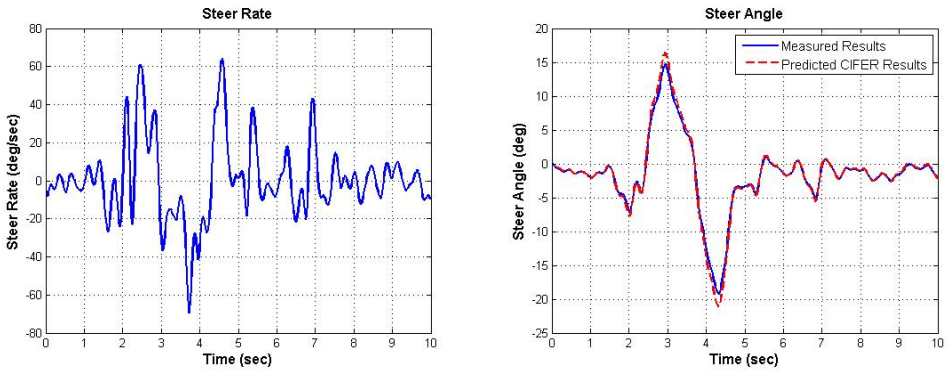

(a) (b)

Figure 5.9: Steer-to-Lean time-domain results a) Steer Rate Input b) Measured and Predicted results for Steer Angle

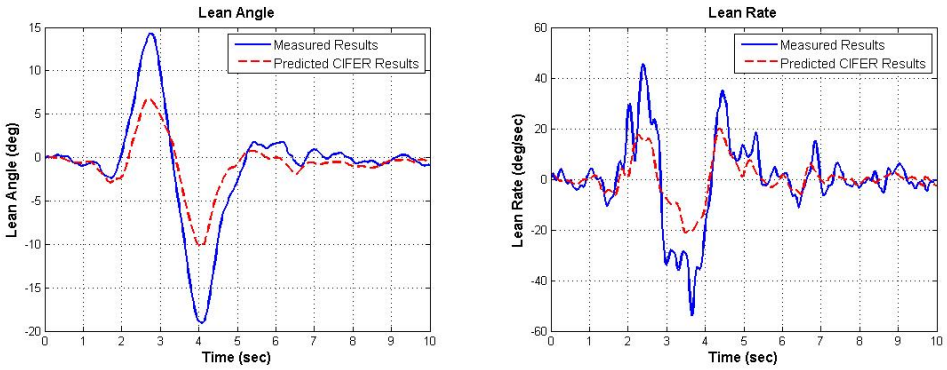

(a) (b)

Figure 5.10: Steer-to-Lean time-domain results a) Measured and Predicted results for Lean Angle b) Measured and Predicted results for Lean Rate

Therefore the time-domain results are shown in the tables (5.3, 5.4, 5.5).

Cost:	TIC value:
5.932	0.36450

Table 5.3: Steer-to-Lean Dynamics VERIFY results for the cost (J_{rms}) and *TIC*.

Identified state derivative biases ($\dot{x_b}$):	Engineering Symbol	Value
Steer Angle	δ	-0.002
Lean Angle	ϕ	3.117
Lean Rate	$\dot{\phi}$	-15.819

Table 5.4: Steer-to-Lean Dynamics VERIFY results for the Identified state derivative biases.

Identified output reference shifts (y_{ref}):	Engineering Symbol	Value
Steer Angle	δ	0.256
Lean Angle	ϕ	0.272
Lean Rate	$\dot{\phi}$	3.169

Table 5.5: Steer-to-Lean Dynamics VERIFY results for the Identified output reference shifts.

Lean-to-Steer Dynamics

The time domain verification predicted results from the DERIVID package is plotted against the measured data. The VERIFY package in the CIFER software used the input of lean rate from a Lean-to-Steer lane change maneuver to establish the predicted output results for lean angle, steer angle, and steer rate.

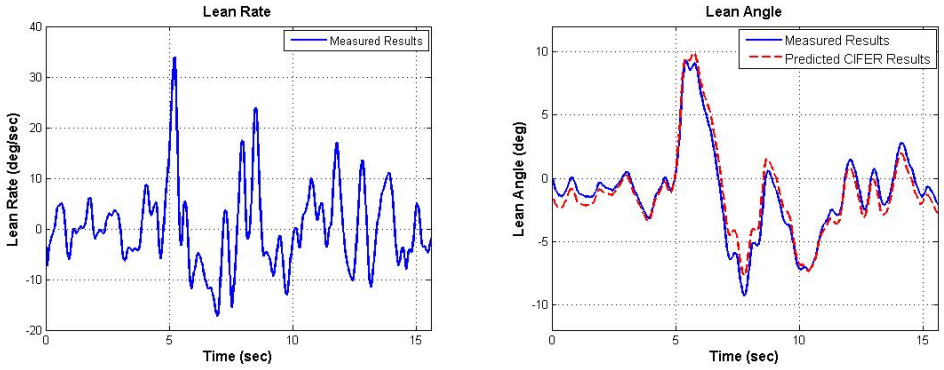

(a) (b)

Figure 5.11: Lean-to-Steer time-domain results a) Lean Rate Input b) Measured and Predicted results for Lean Angle.

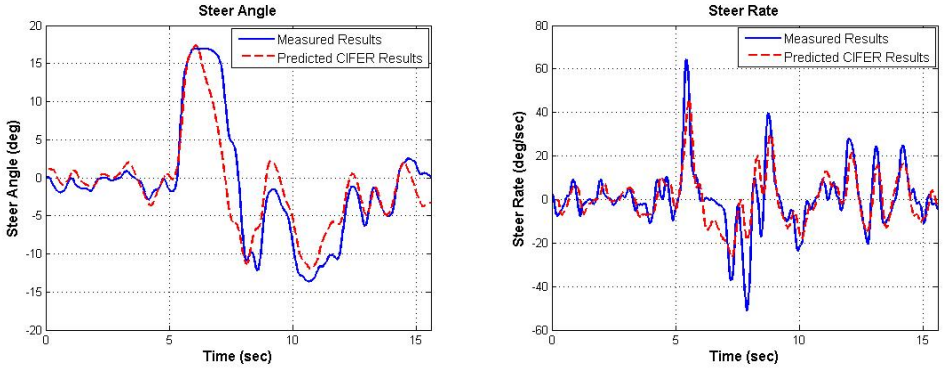

(a) (b)

Figure 5.12: Lean-to-Steer time-domain results a) Measured and Predicted results for Steer Angle b) Measured and Predicted results for Steer Rate.

Therefore the time-domain results are shown in the tables (5.6,5.7,5.8).

Cost:	TIC value:
5.217351	0.3001867

Table 5.6: Lean-to-Steer Dynamics VERIFY results for the cost (J_{rms}) and *TIC*.

Identified state derivative biases ($\dot{x_b}$):	Engineering Symbol	Value
Lean Angle	ϕ	-0.04470828
Steer Angle	δ	-1.793742
Steer Rate	$\dot{\delta}$	11.40507

Table 5.7: Lean-to-Steer Dynamics VERIFY results for the Identified state derivative biases.

Identified output reference shifts (y_{ref}):	Engineering Symbol	Value
Lean Angle	ϕ	-1.195235
Steer Angle	δ	1.311285
Steer Rate	$\dot{\delta}$	-1.488099

Table 5.8: Lean-to-Steer Dynamics VERIFY results for the Identified output reference shifts.

5.5 System Identification of the Empirical Bicycle Model

After identifying the unknown parameters for each reduced model (Steer-to-Lean & Lean-to-Steer) the entire bicycle must also be identified. The Steer-to-Lean Dynamics and Lean-to-Steer Dynamics model equations were determined (3.10 & 3.11). Both of these model equations included unknown parameters from the $[B]$ matrix (equation 3.9). The Steer-to-Lean Dynamics model equation included unknown parameters (b_{31}, b_{32}) from the $[B]$ matrix. And the Lean-to-Steer Dynamics model equation included unknown parameters (b_{41}, b_{42}) from the $[B]$ matrix. The following describes how the unknown parameters from the $[B]$ matrix was determined. Since the Steer-to-Lean reduced model was described the experiments with a rigid rider that only controls the bicycle by applying a steering angle. It was implied that leaning torque ($T_\phi = 0$) by this description. Repeating the Steer-to-Lean Dynamic equation (3.10) from section 3.2 shows the setup of the unknown $[B]$ matrix parameters.

$$\begin{bmatrix} \dot{\phi} \\ \ddot{\phi} \end{bmatrix} = \begin{bmatrix} 0 & 1 \\ a_{31} & a_{33} \end{bmatrix} \begin{bmatrix} \phi \\ \dot{\phi} \end{bmatrix} + \begin{bmatrix} 0 & 0 \\ a_{32} & a_{34} \end{bmatrix} \begin{bmatrix} \delta \\ \dot{\delta} \end{bmatrix} + \begin{bmatrix} 0 & 0 \\ b_{31} & b_{32} \end{bmatrix} \begin{bmatrix} T_\phi \\ T_\delta \end{bmatrix} \tag{5.31}$$

By setting the leaning torque to zero, and after applying matrix multiplication to the equation the results conclude that $b_{31} = 0$. Therefore the only unknown from the Steer-to-Lean Dynamics equation as (b_{32}), since it is dependent on the steering torque input (T_δ).

Likewise, the Lean-to-Steer reduced model was described the experiments with no rider on the bicycle. The experiments involved no rider on the bicycle and were essentially "hands-free". Thus, the bicycle was pushed by applying pressure to the seat and the seat post therefore allowing the steering column to freely oscillate. This implied that there was no external steering torque applied to the bicycle during these experiments. Therefore, steering torque (T_δ) equaled zero. Repeating the Lean-to-Steer Dynamic equation (3.11) from section 3.2 shows the setup of the unknown $[B]$ matrix parameters.

$$\begin{bmatrix} \dot{\delta} \\ \ddot{\delta} \end{bmatrix} = \begin{bmatrix} 0 & 1 \\ a_{42} & a_{44} \end{bmatrix} \begin{bmatrix} \delta \\ \dot{\delta} \end{bmatrix} + \begin{bmatrix} 0 & 0 \\ a_{41} & a_{43} \end{bmatrix} \begin{bmatrix} \phi \\ \dot{\phi} \end{bmatrix} + \begin{bmatrix} 0 & 0 \\ b_{41} & b_{42} \end{bmatrix} \begin{bmatrix} T_\phi \\ T_\delta \end{bmatrix} \tag{5.32}$$

By setting the steering torque to zero, and after implementing matrix multiplication to

the equation the results conclude that $b_{42} = 0$. Therefore the only unknown from the Lean-to-Steer Dynamics equation as (b_{41}), since it is dependent on the leaning torque input (T_ϕ).

Since, the goal is to system identify the Brompton Bicycle we can make assumptions based off the bicycle state-space model equation (3.9) for the unknown parameters for the $[B]$ matrix. In general, the bicycle model equation shows the inverse of the mass matrix $[M^{-1}]$ for the $[B]$ matrix. Thus, assuming that the unknown parameters can be determined by the mass matrix values. These parameters are calculated from the Solidworks model for the Brompton Bicycle and the equations in Appendix A. The resulting values from the $[M^{-1}]$ are included in table (A.2). Thus, the full bicycle model with the known and unknown parameters included is shown as

$$\begin{bmatrix} \dot{\phi} \\ \dot{\delta} \\ \ddot{\phi} \\ \ddot{\delta} \end{bmatrix} = \begin{bmatrix} 0 & 0 & 1 & 0 \\ 0 & 0 & 0 & 1 \\ -6.886 & 2.685 & -4.118 & 1.881 \\ 0.098629 & -0.51823 & 14.314 & -8.6134 \end{bmatrix} \begin{bmatrix} \phi \\ \delta \\ \dot{\phi} \\ \dot{\delta} \end{bmatrix} + \begin{bmatrix} 0 & 0 \\ 0 & 0 \\ 0 & 0.0158 \\ 39.1715 & 0 \end{bmatrix} \begin{bmatrix} T_\phi \\ T_\delta \end{bmatrix} \tag{5.33}$$

With the output equation written with a 4x4 Identity and zeros 4x2 matrices.

Chapter 6

Bicycle Control Models

6.1 Overview of the Bicycle Control Models

The Empirical bicycle model can be shown by implementing the results into the Bicycle Rider Control model (6.1) and the Complete Rider/Vehicle model (6.1) as described in [1]. Hess developed the theoretical control model for the bicycle rider. The original model for the rider originated from a piloting model of his previous work. He used the linearize bicycle control model equation 3.1 to construct feedback loops to stabilize the rider and the bicycle. He developed two control feedback loop systems including the Bicycle Rider Control model and the Complete Rider/Vehicle model [1]. The Bicycle Rider Control model was structured for a roll control, which includes T_δ as an input. These feedback models show how the sensory information of the human can be connected to the dynamics of the bicycle.

The proprioceptive, vestibular, and visual systems are included with reference to the neuromuscular model to show how the rider determines δ, ϕ, and $\dot{\phi}$ during a maneuver. The proprioceptive loop refers to the rider's arms in the muscle spindles and joint angle receptors [1]. The steer angle (δ) is then used in the proportional feedback loop K_δ, which describes the proprioceptive loop of the bicycle. The vestibular loop refers to the sensors in the inner ear specifically in the semicircular canals [1]. The lean rate ($\dot{\phi}$) is then used in the proportional feedback loop $K_{\dot{\phi}}$, which describes the vestibular loop of the bicycle. Lastly, the visual loop refers to the rider's eyes [1]. The lean angle

(ϕ) is then used in the proportional feedback loop K_ϕ, which describes the visual loop of the bicycle. The Complete Rider/Vehicle model augments the visual system with respect to how the rider and vehicle are connected to complete the maneuver in terms of heading (Ψ) and lateral deviation (y). In addition, ϕ, δ, $\dot{\phi}$, $\dot{\delta}$, Ψ, and y results that are extracted from these models help understand the rider's control strategy for the experiment.

The neuromuscular model describes the rider's arms and legs that produce the control inputs. The control inputs from the rider's arms and legs help stabilize the bicycle dynamics during a maneuver. This model is described as [1],

$$G_{nm_b} = \frac{30^2}{s^2 + 2(0.707)30s + 30^2} \tag{6.1}$$

The addition of the neuromuscular model helps stabilize the bicycle since it reduces the bandwidth from the gain K_δ to the output of steer angle.

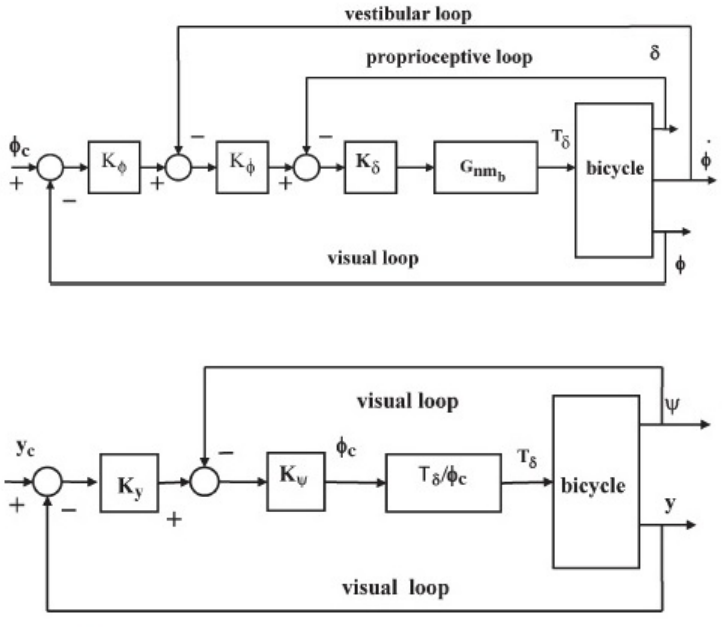

Figure 6.1: Bicycle feedback loop diagrams a) Bicycle Rider Control model b) Complete Rider/Vehicle Control model [1].

6.2 Implementing the Empirical Model into the Control Models

The Empirical model was inserted into the control models as described above. The reference input (y_r) implemented the rear wheel position of the y-axis results from a Steer-to-Lean lane change maneuver. The feedback gains (K_δ, K_ϕ, $K_{\dot{\phi}}$, K_Ψ; K_y) can be determined from this reference input respective to the implemented bicycle model. The goal is to validate the model by comparing the simulated and actual experimental results for these feedback gain values and the bicycle model.

6.2.1 Model Structure

The Complete Rider/Vehicle model includes the outputs of heading (Ψ) and lateral deviation (y). Additional equations are necessary to create these outputs. These equations are referenced from [1].

$$\dot{\Psi} = \frac{v\delta + c\delta}{w} cos(\lambda) \tag{6.2}$$

$$y = y_r + w\Psi - c\delta cos(\lambda) \tag{6.3}$$

$$\dot{y_r} = v\Psi \tag{6.4}$$

With the addition of these equations the Empirical model can be written in a $6x6$ matrix format. Since the Complete Rider/Vehicle model involves only an input of steering torque, then leaning torque is automatically equal zero. The state vector includes the lean angle (ϕ), steering angle (δ), lean rate ($\dot{\phi}$), steering rate ($\dot{\delta}$), heading (Ψ), and lateral deviation (y). The state space equation is written as

$$\begin{bmatrix} \dot{\phi} \\ \dot{\delta} \\ \ddot{\phi} \\ \ddot{\delta} \\ \dot{\Psi} \\ \dot{y} \end{bmatrix} = \begin{bmatrix} 0 & 0 & 1 & 0 & 0 & 0 \\ 0 & 0 & 0 & 1 & 0 & 0 \\ a_{31} & a_{32} & a_{33} & a_{34} & 0 & 0 \\ a_{41} & a_{42} & a_{43} & a_{44} & 0 & 0 \\ 0 & \frac{v}{w}cos(\lambda) & 0 & \frac{c}{w}cos(\lambda) & 0 & 0 \\ 0 & vcos(\lambda) & 0 & 0 & v & 0 \end{bmatrix} \begin{bmatrix} \phi \\ \delta \\ \dot{\phi} \\ \dot{\delta} \\ \Psi \\ y \end{bmatrix} + \begin{bmatrix} 0 & 0 \\ 0 & 0 \\ b_{31} & b_{32} \\ b_{41} & b_{42} \\ 0 & 0 \\ 0 & 0 \end{bmatrix} \begin{bmatrix} 0 \\ T_\delta \end{bmatrix} \tag{6.5}$$

Since the reference input (y_r) is from the rear wheel position in the y-axis, the velocity (v) is then applied from the rear wheel (v_r). The average rear wheel velocity was applied into this equation since during the lane change maneuver there was not a constant velocity. The output equation consists of a $6x6$ Identity matrix and $6x1$ zero vector. Both values (b_{32} and b_{42}) from $[M^{-1}]$ of the Solidworks Brompton model are included into this equation for the Empirical model since the steering torque input relies on the mass moments of inertia & properties along the steering axis and for the whole bicycle along the z-axis. Therefore, the equation can be written with all values included as

$$\begin{bmatrix} \dot{\phi} \\ \dot{\delta} \\ \ddot{\phi} \\ \ddot{\delta} \\ \dot{\Psi} \\ \dot{y} \end{bmatrix} = \begin{bmatrix} 0 & 0 & 1 & 0 & 0 & 0 \\ 0 & 0 & 0 & 1 & 0 & 0 \\ -6.8858 & 2.6855 & -4.1179 & 1.8809 & 0 & 0 \\ 0.9863 & -0.5182 & 14.3140 & -8.6134 & 0 & 0 \\ 0 & 3.0439 & 0 & 0.0271 & 0 & 0 \\ 0 & 3.2266 & 0 & 0 & 3.3740 & 0 \end{bmatrix} \begin{bmatrix} \phi \\ \delta \\ \dot{\phi} \\ \dot{\delta} \\ \Psi \\ y \end{bmatrix} + \begin{bmatrix} 0 \\ 0 \\ -0.3607 \\ 39.1715 \\ 0 \\ 0 \end{bmatrix} \begin{bmatrix} T_\delta \end{bmatrix} \tag{6.6}$$

Since both of the reduced models results had stable transfer functions thus the overall $6x6$ $[A]$ matrix has stable poles. In general, if the state-space matrix is not stable the feedback gains can be used to stabilize the system. For the Empirical bicycle model, we wish to determine the feedback gains to simulate the results as close to the actual experimental results.

Controllability and Observability

Before determining the feedback gains (K_δ, K_ϕ, $K_{\dot{\phi}}$, K_Ψ; K_y) for the Complete Rider/Vehicle model we need to make sure the state-space matrix is controllable and observable. To determine if the state-space matrix is controllable we use this definition [8],

$$C = [B \;\; AB \;\; A^2B \;\; ... \;\; A^{n-1}B] \tag{6.7}$$

where, $[A]$ and $[B]$ are the defined matrices for the system. The rank of the controllable matrix is also determined. The rank of the controllable matrix must match the rank of the system. To determine if the state-space matrix is observable we use this definition

[8],

$$O = \begin{bmatrix} C \\ CA \\ CA^2 \\ ... \\ CA^{n-1} \end{bmatrix} \tag{6.8}$$

where, [A] and [C] are the defined matrices for the system. The rank of the [C] matrix must be equal to the rank of O to be observable.

6.2.2 Linear Quadratic Regulation Method

To obtain the optimal regulation for the feedback gains (K_δ, K_ϕ, $K_{\dot{\phi}}$, K_Ψ; K_y) for the Complete Rider/Vehicle model we need to use a Linear Quadratic Regulation (LQR). We can obtain the regulator gain matrix K by minimizing the cost (J_{LQR}). Thus, from the Appendix (B.5) the most general form of the LQR is

$$J_{LQR} \; = \; \int_0^\infty x'Qx \; + \; u'Ru \; + \; 2x'Nudt \tag{6.9}$$

where, Q and R are symmetric positive-definite matrices. From the criterion (B.12)

$$z \; = \; Gx \; + \; Hu \tag{6.10}$$

is a special form of 6.9 then Q, R, and N can be written other formats. These formats include

$$Q \; = \; G'QG \quad R \; = \; H'H \; + \; pI \quad N \; = \; G'QH \tag{6.11}$$

In addition to solving for the LQR general equation(6.9), it requires a solution to the Algebraic Riccati Equation (ARE) [8] which states

$$A'P \; + \; PA \; + \; Q \; - \; (PB \; + \; N)R^{-1}(B'P \; + \; N') = 0 \tag{6.12}$$

The solution here is P it is dependent on Q, R, and N of the system. In MATLAB [9], one can use the command 'lqr' to obtain the solution P to the Algebraic Riccati Equation. The equation for this command [8],

$$[K, P, E] \; = \; lqr(A, B, Q, R, N) \tag{6.13}$$

It also computes the negative feedback optimal state feedback gain K. This K minimizes the LQR general form equation 6.9 for the continuous time process. In addition it also returns the poles E to the closed loop system, [8]

$$\dot{x} \; = \; (A \; - \; BK)x \tag{6.14}$$

For the choices for Q and R for our system we used Bryson's rule to help us choose the simplest values. By selecting Q and R diagonals with in Bryson's rule design [8],

$$Q_{ii} \; = \; \frac{1}{maximum \;\; acceptable \;\; value \;\; of \;\; z_i^2}, \;\; for \;\; i \in \{1, 2, ..., l\} \tag{6.15}$$

$$R_{jj} \; = \; \frac{1}{maximum \;\; acceptable \;\; value \;\; of \;\; u_j^2}, \;\; for \;\; j \in \{1, 2, ..., k\} \tag{6.16}$$

This corresponds to the criterion of the general equation 6.9. Bryson's rule is a good starting point for trial and error iterative design procedure for obtaining the desirable properties for the closed loop system.

6.2.3 Determining the Gains for the Empirical Bicycle Model

In order to determine the gains for the Empirical Bicycle Model we needed to use the Complete Rider/Vehicle model [1]. The neuromuscular model 6.1 was included into the Complete Rider/Vehicle model to determined the necessary gains. We expanded the Complete Rider/Vehicle model to incorporate all of the gains (K_δ, K_ϕ, $K_{\dot{\phi}}$, K_Ψ; K_y) for the 6x6 system by remodeling it into a cascaded formated. This cascaded format includes an additional gain $K_{\dot{\delta}}$, which was not explicitly accounted for in the original model. By using this format, we had to use the MATLAB [9] command 'connect' to essentially piece together the cascaded system. The 'connect' command interconnects block diagrams of the dynamic systems. In addition, by using this command an overall cascaded Simulink model was not necessary to show how the gains were connected to the entire dynamic system.

The Q matrix for the Empirical Bicycle Model is defined as

$$Q = \begin{bmatrix} \frac{1}{(x_1)^2} & 0 & 0 & 0 & 0 & 0 \\ 0 & \frac{1}{(x_2)^2} & 0 & 0 & 0 & 0 \\ 0 & 0 & \frac{1}{(x_3)^2} & 0 & 0 & 0 \\ 0 & 0 & 0 & \frac{1}{(x_4)^2} & 0 & 0 \\ 0 & 0 & 0 & 0 & \frac{1}{(x_5)^2} & 0 \\ 0 & 0 & 0 & 0 & 0 & \frac{1}{(x_6)^2} \end{bmatrix} \tag{6.17}$$

where, each value of x_n (for $n = 1, 2, 3, ..., 6$) is determined by trial and error. The R matrix is defined as a single value since the size of the $[B]$ is a $6x1$ vector.

$$R = \left[\frac{1}{(u_1)^2}\right] \tag{6.18}$$

where, the value of (u_1) is also determined by trial and error. This is to determine the best results for the gains for the system. In conjunction with the matrices 6.6 the feedback gain matrix K can be determined. This matrix is defined as

$$K_{lqr} = [K_{lqr}(1,1) \;\; K_{lqr}(1,2) \;\; K_{lqr}(1,3) \;\; K_{lqr}(1,4) \;\; K_{lqr}(1,5) \;\; K_{lqr}(1,6)] \tag{6.19}$$

Since the cascaded version of the Complete Rider/Vehicle model is used the K_{lqr} gains are in a nested format. The nested format defines the particular gains for the model.

$$K_{\dot{\delta}} = K_{lqr}(1,4) \tag{6.20}$$

$$K_{\delta} = \frac{K_{lqr}(1,2)}{K_{lqr}(1,4)} \tag{6.21}$$

$$K_{\dot{\phi}} = \frac{K_{lqr}(1,3)}{K_{lqr}(1,2)} \tag{6.22}$$

$$K_{\phi} = \frac{K_{lqr}(1,1)}{K_{lqr}(1,3)} \tag{6.23}$$

$$K_{\psi} = \frac{K_{lqr}(1,5)}{K_{lqr}(1,1)} \tag{6.24}$$

$$K_{y} = \frac{K_{lqr}(1,6)}{K_{lqr}(1,5)} \tag{6.25}$$

Empirical Model Results

The reference input from the rear wheel position in the y-axis from the Steer-to-Lean lane change maneuver is simulated for each of the outputs from the determined gains. In conjunction with the matrices 6.6 the feedback gain matrix K can be determined. Thus, the results for these gains are:

$$\begin{bmatrix} K_{\dot{\delta}} \\ K_{\delta} \\ K_{\dot{\phi}} \\ K_{\phi} \\ K_{\psi} \\ K_{y} \end{bmatrix} = \begin{bmatrix} 0.6789 \\ 4.7592 \\ 1.0055 \\ 8.2277 \\ 0.6900 \\ 0.4300 \end{bmatrix} \tag{6.26}$$

The following results from these gains are given.

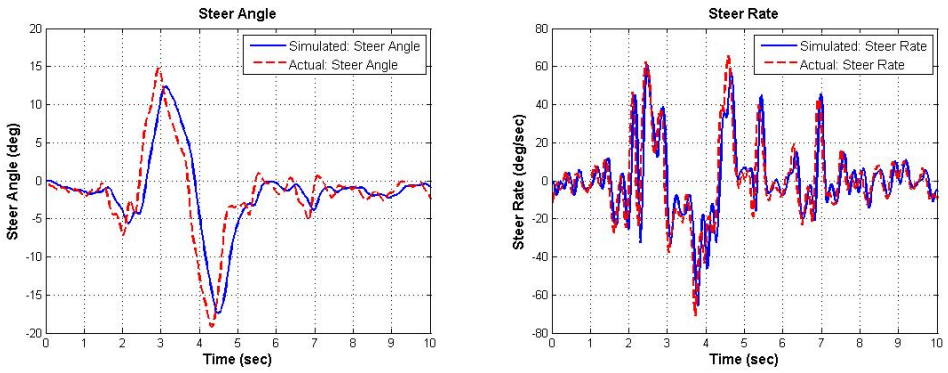

(a) (b)

Figure 6.2: Simulated and Actual results for a) Steer Angle b) Steer Rate.

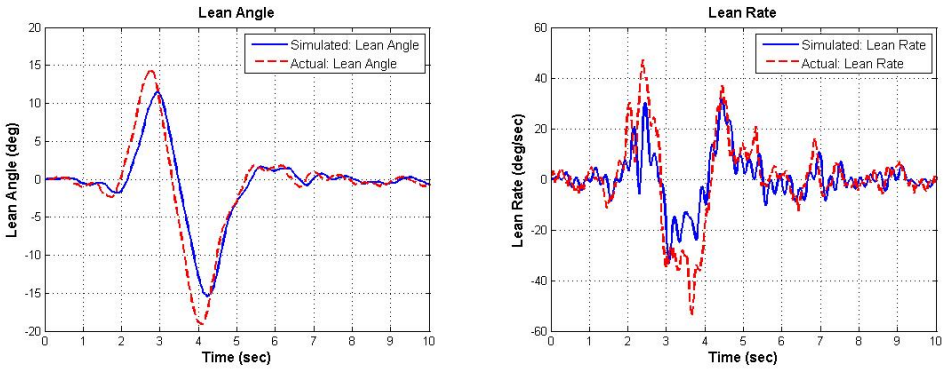

(a) (b)

Figure 6.3: Simulated and Actual results for a) Lean Angle b) Lean Rate.

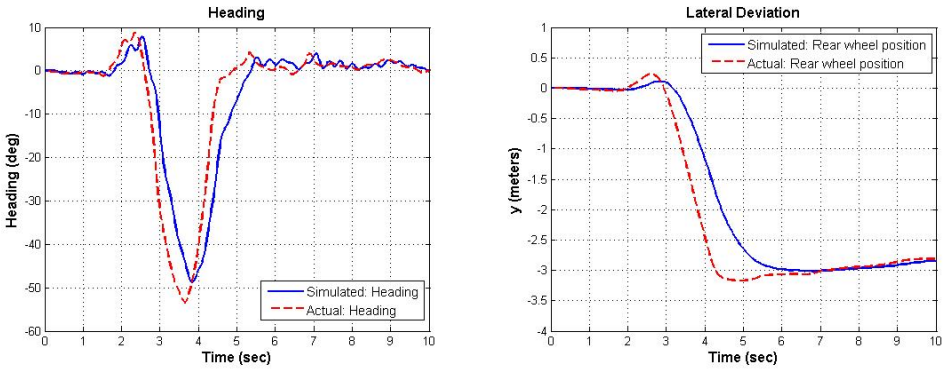

(a) (b)

Figure 6.4: Simulated and Actual results for a) Heading b) Lateral Deviation.

6.3 Implementing the Theoretical Model into the Control Models

The Theoretical model was inserted into the control models as described 6.1 and 6.1. The reference input (y_r) implemented rear wheel position of the y-axis results from a Steer-to-Lean lane change maneuver. The feedback gains (K_δ, K_ϕ, $K_{\dot{\phi}}$, K_Ψ; K_y) can be determined from this reference input respective to the implemented bicycle model. The goal is to show the behavior of theoretical model by comparing the simulated and actual experimental results. The feedback gains values from the LQR controller are used to show this comparison.

6.3.1 Model Structure

The Theoretical model also incorporates 6.3, 6.4, 6.2 to form the 6x6 matrix format. Since the Complete Rider/Vehicle model involves only an input of steering torque, then leaning torque is automatically equal zero. The state vector includes the lean angle (ϕ), steering angle (δ), lean rate ($\dot{\phi}$), steering rate ($\dot{\delta}$), heading (Ψ), and lateral deviation (y). The state space equation is written as

$$\begin{bmatrix} \dot{\phi} \\ \dot{\delta} \\ \ddot{\phi} \\ \ddot{\delta} \\ \dot{\Psi} \\ \dot{y} \end{bmatrix} = \begin{bmatrix} 0 & 0 & 1 & 0 & 0 & 0 \\ 0 & 0 & 0 & 1 & 0 & 0 \\ -Nn(1,1) & -Nn(1,2) & -Pn(1,1) & -Pn(1,2) & 0 & 0 \\ -Nn(2,1) & -Nn(2,2) & -Pn(2,1) & -Pn(2,1) & 0 & 0 \\ 0 & \frac{v}{w}cos(\lambda) & 0 & \frac{c}{w}cos(\lambda) & 0 & 0 \\ 0 & vcos(\lambda) & 0 & 0 & v & 0 \end{bmatrix} \begin{bmatrix} \phi \\ \delta \\ \dot{\phi} \\ \dot{\delta} \\ \Psi \\ y \end{bmatrix} + \begin{bmatrix} 0 & 0 \\ 0 & 0 \\ b_{31} & b_{32} \\ b_{41} & b_{42} \\ 0 & 0 \\ 0 & 0 \end{bmatrix} \begin{bmatrix} 0 \\ T_\delta \end{bmatrix} \tag{6.27}$$

Since the reference input is from the rear wheel position in the y-axis, the velocity (v) is then applied from the rear wheel (v_r). The average rear wheel velocity was applied into this equation since during the lane change maneuver there was not a constant velocity. The output equation consists of a $6x6$ Identity matrix and $6x1$ zero vector. Therefore

the equation can be written with all values included as

$$\begin{bmatrix} \dot{\phi} \\ \dot{\delta} \\ \ddot{\phi} \\ \ddot{\delta} \\ \dot{\Psi} \\ \dot{y} \end{bmatrix} = \begin{bmatrix} 0 & 0 & 1 & 0 & 0 & 0 \\ 0 & 0 & 0 & 1 & 0 & 0 \\ 8.0971 & -9.0820 & -0.1077 & -0.9052 & 0 & 0 \\ 46.7949 & 24.4189 & 11.7010 & -21.0769 & 0 & 0 \\ 0 & 3.0439 & 0 & 0.0271 & 0 & 0 \\ 0 & 3.2266 & 0 & 0 & 3.3740 & 0 \end{bmatrix} \begin{bmatrix} \phi \\ \delta \\ \dot{\phi} \\ \dot{\delta} \\ \Psi \\ y \end{bmatrix} + \begin{bmatrix} 0 \\ 0 \\ -0.3607 \\ 39.1715 \\ 0 \\ 0 \end{bmatrix} \begin{bmatrix} T_\delta \end{bmatrix} \tag{6.28}$$

Since the theoretical model was initially unstable it was difficult to obtain the corresponding gains for the LQR controller. This was especially shown with the outputs for steer angle (δ) and the steer rate ($\dot{\delta}$).

A feedback model for the Theoretical model 4x4 system was used to stabilize this system. The feedback model for the 4x4 system used the MATLAB [9] command 'place' for the pole placement design. The desired pole locations included $-21.9694 + 0.0000i$, $-3.0510 + 0.0000i$, $-1.9179 + 2.3689i$; $-1.9179 - 2.3689i$. The input of the desired pole locations created a feedback gain matrix K_{fbk} for this 4x4 system. The feedback model state equation is described as

$$\dot{x} = (A - (B * K_{fbk}))x \ + \ Bu \tag{6.29}$$

with the output as

$$y = Cx \ + \ Du \tag{6.30}$$

The feedback gain matrix K_{fbk} includes four gains to stabilize the 4x4 system. This feedback gain K_{fbk} is written as

$$K_{fbk} = \begin{bmatrix} 1431.90 & -814.8 & 308.8 & -126.4 \\ 14.30 & -5.20 & 3.10 & -1.10 \end{bmatrix} \tag{6.31}$$

K_{fbk} is written in completeness where the top row refer to the input of leaning torque (T_ϕ) and the bottom row refers to the input of steering torque (T_δ). The focus is only on the bottom row of K_{fbk} since we have already defined leaning torque (T_ϕ) to be zero.

Therefore, the Theoretical model (4x4) can be rewritten as

$$\begin{bmatrix} \dot{\phi} \\ \dot{\delta} \\ \ddot{\phi} \\ \ddot{\delta} \end{bmatrix} = \begin{bmatrix} 0 & 0 & 1.0000 & 0 \\ 0 & 0 & 0 & 1.0000 \\ -9.355 & 1.925 & -3.86 & 0.7074 \\ 1.945 & -66.96 & 0.711 & -25 \end{bmatrix} + \begin{bmatrix} \phi \\ \delta \\ \dot{\phi} \\ \dot{\delta} \end{bmatrix} \begin{bmatrix} 0 & 0 \\ 0 & 0 \\ 0.0158 & -0.3607 \\ -0.3607 & 39.1715 \end{bmatrix} \begin{bmatrix} 0 \\ T_\delta \end{bmatrix} \tag{6.32}$$

Thus, we can now write the Theoretical model in the 6x6 matrix format that includes the stabilized 4x4 system. This is written as

$$\begin{bmatrix} \dot{\phi} \\ \dot{\delta} \\ \ddot{\phi} \\ \ddot{\delta} \\ \dot{\Psi} \\ \dot{y} \end{bmatrix} = \begin{bmatrix} 0 & 0 & 1 & 0 & 0 & 0 \\ 0 & 0 & 0 & 1 & 0 & 0 \\ -9.355 & 1.925 & -3.86 & 0.7074 & 0 & 0 \\ 1.945 & -66.96 & 0.711 & -25 & 0 & 0 \\ 0 & 3.0439 & 0 & 0.0271 & 0 & 0 \\ 0 & 3.2266 & 0 & 0 & 3.3740 & 0 \end{bmatrix} \begin{bmatrix} \phi \\ \delta \\ \dot{\phi} \\ \dot{\delta} \\ \Psi \\ y \end{bmatrix} + \begin{bmatrix} 0 \\ 0 \\ -0.3607 \\ 39.1715 \\ 0 \\ 0 \end{bmatrix} \begin{bmatrix} T_\delta \end{bmatrix} \tag{6.33}$$

6.3.2 Determining Gains for the Theoretical Model

The sections that describe the Linear Quadratic Regulation method 6.2.2, controllability and observability 6.2.1 also apply to the Theoretical model.

In order to determine the gains for the Theoretical Model we needed to use the Complete Rider/Vehicle model [1]. The neuromuscular model 6.1 was included into the Complete Rider/Vehicle model to determined the necessary gains. We expanded the Complete Rider/Vehicle model to incorporate all of the gains (K_δ, K_ϕ, $K_{\dot{\phi}}$, K_Ψ; K_y) for the 6x6 system by remodeling it into a cascaded formated. This cascaded format includes an additional gain $K_{\dot{\delta}}$, which was not explicitly accounted for in the original model. By using this format, we had to use the MATLAB [9] command 'connect' to essentially piece together the cascaded system. The 'connect' command interconnects block diagrams of the dynamic systems. In addition, by using this command an overall cascaded Simulink model was not necessary to show how the gains were connected to the entire dynamic system.

The Q matrix for the Theoretical Bicycle Model is defined as

$$Q = \begin{bmatrix} \frac{1}{(x_1)^2} & 0 & 0 & 0 & 0 & 0 \\ 0 & \frac{1}{(x_2)^2} & 0 & 0 & 0 & 0 \\ 0 & 0 & \frac{1}{(x_3)^2} & 0 & 0 & 0 \\ 0 & 0 & 0 & \frac{1}{(x_4)^2} & 0 & 0 \\ 0 & 0 & 0 & 0 & \frac{1}{(x_5)^2} & 0 \\ 0 & 0 & 0 & 0 & 0 & \frac{1}{(x_6)^2} \end{bmatrix} \tag{6.34}$$

where, each value of x_n (for $n = 1, 2, 3, ..., 6$) is determined by trial and error. The R matrix is defined as a single value since the size of the $[B]$ is a $6x1$ vector.

$$R = \left[\frac{1}{(u_1)^2}\right] \tag{6.35}$$

where, the value of (u_1) is also determined by trial and error. This is to determine the best results for the gains for the system. In conjunction with the matrices 6.33 the feedback gain matrix K can be determined. This matrix is defined as

$$K_{lqr} = [K_{lqr}(1,1) \;\; K_{lqr}(1,2) \;\; K_{lqr}(1,3) \;\; K_{lqr}(1,4) \;\; K_{lqr}(1,5) \;\; K_{lqr}(1,6)] \tag{6.36}$$

Since the cascaded version of the Complete Rider/Vehicle model is used the K_{lqr} gains are in a nested format. The nested format defines the particular gains for the model.

$$K_{\dot{\delta}} = K_{lqr}(1,4) \tag{6.37}$$

$$K_{\delta} = \frac{K_{lqr}(1,2)}{K_{lqr}(1,4)} \tag{6.38}$$

$$K_{\dot{\phi}} = \frac{K_{lqr}(1,3)}{K_{lqr}(1,2)} \tag{6.39}$$

$$K_{\phi} = \frac{K_{lqr}(1,1)}{K_{lqr}(1,3)} \tag{6.40}$$

$$K_{\psi} = \frac{K_{lqr}(1,5)}{K_{lqr}(1,1)} \tag{6.41}$$

$$K_{y} = \frac{K_{lqr}(1,6)}{K_{lqr}(1,5)} \tag{6.42}$$

Theoretical Model Results

In conjunction with the matrices in 6.33 the feedback gain matrix K can be determined. Thus, the results for these gains are:

$$\begin{bmatrix} K_{\dot{\delta}} \\ K_{\delta} \\ K_{\dot{\phi}} \\ K_{\phi} \\ K_{\psi} \\ K_{y} \end{bmatrix} = \begin{bmatrix} 2.1555 \\ 5.0079 \\ 2.2800 \\ 14.5000 \\ 0.5000 \\ 0.3290 \end{bmatrix} \tag{6.43}$$

The following results from these gains are given.

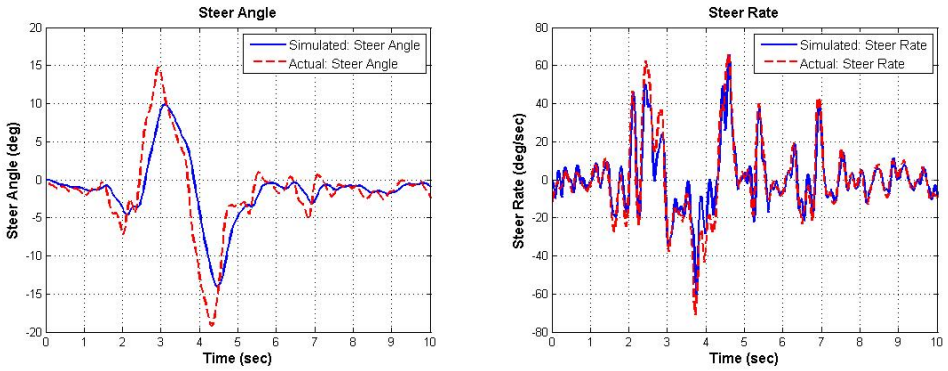

(a) (b)

Figure 6.5: Simulated and Actual results for a) Steer Angle b) Steer Rate.

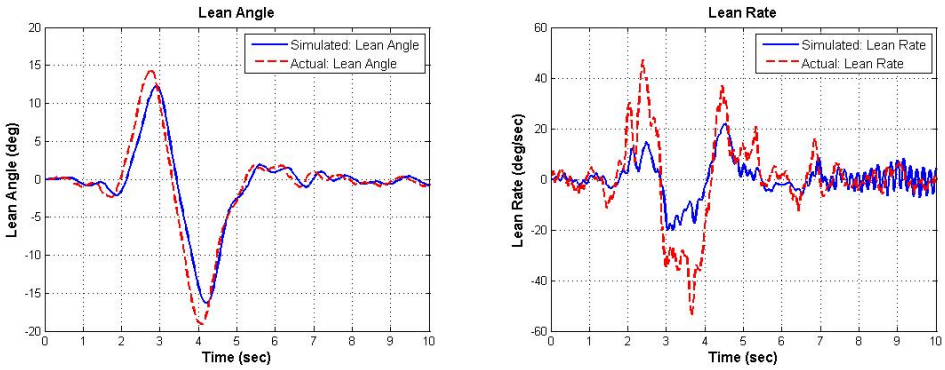

(a) (b)

Figure 6.6: Simulated and Actual results for a) Lean Angle b) Lean Rate.

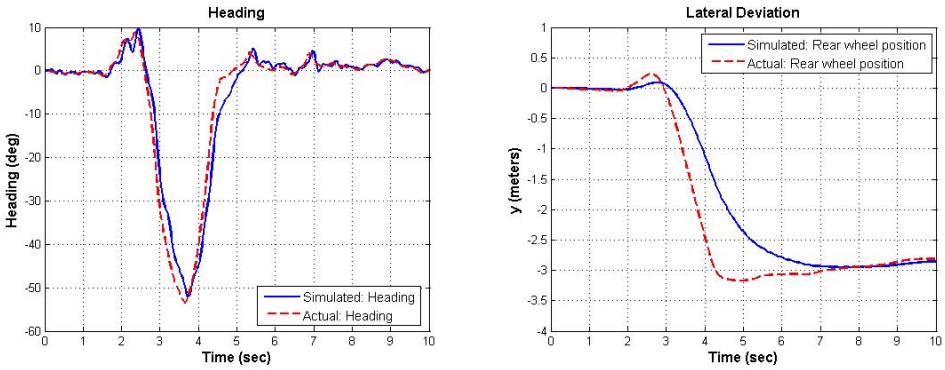

(a) (b)

Figure 6.7: Simulated and Actual results for a) Heading b) Lateral Deviation.

6.4 Comparison of the Empirical and Theoretical Models

Both of the Empirical and Theoretical models gains (K_δ, K_ϕ, $K_{\dot{\phi}}$, K_Ψ; K_y) are determined by a LQR controller in 6.26 and 6.43. As previously stated these gains were determined by using the reference input (y_r) implemented from the rear wheel position of the y-axis results from a Steer-to-Lean lane change maneuver. As expected the gains for both models are different. One of the contributing factors to these different gains is due to how the [A] matrices are defined. The Empirical model values were obtained from the state-space model derivatives in the system identification process for the two reduced models Steer-to-Lean dynamics and Lean-to-Steer dynamics. The Theoretical model values were determined by using the mass moments of inertia and properties based on the Solidworks model of the Brompton bicycle (2.1) and the equations described in Appendix A. After the application of the feedback loop on the 4x4 Theoretical model system the simulated results from the LQR controller were better.

Even though the [A] matrices were defined differently for each model, there are similarities in gains that were determined by the LQR controller. It is interesting that K_δ and K_ϕ gains resulted in bigger values for both models. The simulated results for steer angle (δ) from the proportional feedback loop (K_δ) for both models are close to the actual experimental results (6.2.3 and 6.3.2). The simulated results for lean angle (ϕ) from the proportional feedback loop (K_ϕ) for both models are close to the actual experimental results (6.2.3 and 6.3.2). The other values for the gains ($K_{\dot{\phi}}$, K_Ψ, K_y; $K_{\dot{\delta}}$) were small in comparison. The gains K_δ and K_ϕ are included into the Bicycle Rider control model (6.1 from [1]). The steer angle (δ) is then used in the proportional feedback loop K_δ, which describes the proprioceptive loop of the bicycle. The lean angle (ϕ) is then used in the proportional feedback loop K_ϕ, which describes the visual loop of the bicycle. The lean and steer angle results based from these gains (K_δ and K_ϕ) help understand the rider's control strategy for stabilizing the bicycle during an experiment.

Chapter 7

Conclusion

The Brompton bicycle platform described the physical characteristics, instrumentation, and bicycle state estimator. The bicycle model equation, the determination of the mass moments of inertia, and properties setup for the Whipple bicycle in 3 was used similarly for the Brompton bicycle. The model setup for system identification was shown in detail for the Steer-to-Lean dynamics and Lean-to-Steer dynamics. These were defined as reduced order models that did not include any external torques. The Steer-to-Lean model was shown with a steer rate input. The Lean-to-Steer model was shown with a lean rate input. Experimental results were shown for a variety of maneuvers for the bicycle. The system identification of the Brompton bicycle was shown using the CIFER software. The frequency response, state-space derivatives, and time domain results were determined for the Steer-to-Lean dynamics and Lean-to-Steer dynamics models. The Empirical model was derived in the system identification section. This incorporated the Steer-to-Lean dynamics and Lean-to-Steer dynamics and the mass properties of the actual bicycle. The Empirical model was further validated in the bicycle control models by obtaining various feedback gains by a LQR controller. In addition, the Theoretical model was shown as a comparison to the Empirical model in the bicycle control models.

There were many challenges in using the Steer-to-Lean and Lean-to-Steer reduced models. These included setting the proper length for the experiment and trying to stay within the particular guidelines. It was difficult to achieve a similar velocity for the

Lean-to-Steer dynamics experiments in relation to the Steer-to-Lean dynamic experiment. Since there was no rider on the bicycle for the Lean-to-Steer dynamics experiments this increased the notion of instability.

The future goals are to revise the instrumentation of the bicycle to include a lean torque sensor to the seat post, a steering torque sensor to the handlebars, implement a Go-Pro Hero 3 video camera attached to a gimbaled mount to record the view from the bicycle, and to have the rider wear Gaze Tracking Glasses during a maneuver. In addition, we would like to model the bicycle in a 3D simulation to see how the real rider accomplished the turn to avoid the obstacle. The Gaze Tracking Glasses measurements obtained from SensoMotoric Instruments (SMI) software program can also be included into this 3D simulation. The human can be modeled into the simulation by obtaining accurate measurements of the body and how it moves.

The human subject can be modeled by attaching several strategically placed retro-reflective markers to the person's clothing to measure the movements during an experiment with the bicycle. The VICON cameras will analyze the movements of the retro-reflective markers on the person and can determine the vectors for each movement. Relationships between these vectors obtained from the VICON cameras and VICON tracker software program can provide an understanding to the human sensory information (visual, proprioceptive; vestibular) systems in order to control the bicycle to avoid an obstacle during a trajectory.

References

[1] Ronald Hess, Jason Keith Moore, and Mont Hubbard. Modeling the manually controlled bicycle. *Systems, Man and Cybernetics, Part A: Systems and Humans, IEEE Transactions on*, 42(3):545–557, 2012.

[2] David V Herlihy. *Bicycle: the History*. Yale University Press, 2004.

[3] JP Meijaard, Jim M Papadopoulos, Andy Ruina, and Arend L Schwab. Linearized dynamics equations for the balance and steer of a bicycle: a benchmark and review. *Proceedings of the Royal Society A: Mathematical, Physical and Engineering Science*, 463(2084):1955–1982, 2007.

[4] Mark B Tischler and Robert K Remple. Aircraft and rotorcraft system identification. *AIAA Education Series. American Institute of Aeronautics and Astronautics, New York*, 2006.

[5] JP Meijaard, Jim M Papadopoulos, Andy Ruina, and AL Schwab. Supplementary appendices. *Proceedings of the Royal Society Series A*, 2007.

[6] Monique Hladun, Vishnuu Mallik, and Bérénice Mettler. Bicycle instrumentation and preliminary system identification modeling. Presented at the 2014 AIAA Region V Student Paper Conference, April 2014.

[7] MB Tischler and Mavb G Cauffman. Cifer version 2.1, comprehensive identification from frequency responses, an interactive facility for system identification and verification. *Sterling Software, Palo Alto, CA*, 1994.

[8] João P Hespanha. *Linear Systems Theory*. Princeton University Press, 2009.

[9] Michael Grant, Stephen Boyd, and Yinyu Ye Cvx. Matlab software for disciplined convex programming. *Online accessiable: http://stanford. edu/boyd/cvx*, 2008.

Appendix A

Bicycle Coefficient Equations

The coefficient equations are comprised of the mass moments of inertia and physical properties of the bicycle. The following are the definitions of total mass and centers of mass based on the physical description of bicycle (figure 3). The bicycle is divided into four sections including the front frame, body assembly, rear wheel, and the front wheel. The front frame (including the fork and steering column) is denoted by "H". The body assembly (including the rider's body and rear bicycle frame) is denoted by "B". The rear wheel is denoted by "R". The front wheel is denoted by "F". Thus, the total assembly is denoted by "T". Each of these sub-assemblies and total assembly are reflected about the global axes. The axes are denoted at the rear wheel of the bicycle in figure 3. These axes are shown with the x-axis is in line with the bicycle, the z-axis is positive downward, and the y-axis is positive out of the page. All of these equations are referenced from [3].

Total mass:

$$m_T = m_R + m_B + m_H + m_F \tag{A.1}$$

Center of mass (x-direction):

$$x_T = \frac{x_B m_B + x_H m_H + w * m_F}{m_T} \tag{A.2}$$

Center of mass (z-direction):

$$z_T = \frac{-r_R m_R + z_B m_B + z_H m_H - r_F m_F}{m_T} \tag{A.3}$$

Mass moments of inertia and products of inertia defined for the whole system.

$$I_{Txx} = I_{Rxx} + I_{Bxx} + I_{Hxx} + I_{Fxx} + m_R(r_R)^2 + m_B(r_B)^2 + m_H(r_H)^2 + m_F(r_F)^2 \tag{A.4}$$

$$I_{Txz} = I_{Bxz} + I_{Hxz} - m_B x_B z_B - m_H x_H z_H + m_F w r_F \tag{A.5}$$

Noting that rear and front wheel moment of inertia are defined as:

$$I_{Rzz} = I_{Rxx} \;\; and \;\; I_{Fzz} = I_{Fxx} \tag{A.6}$$

$$I_{Tzz} = I_{Rzz} + I_{Bzz} + I_{Hzz} + I_{Fzz} + m_B(x_B)^2 + m_H(x_H)^2 + m_F(w)^2 \tag{A.7}$$

Total masses, center of masses, and mass moments of inertia are defined in a similar manner for the front assembly (denoted by "A"). Notice how the total front assembly includes the handlebars and the front wheel.

$$m_A = m_H + m_F \tag{A.8}$$

$$x_A = \frac{(x_H m_H + w m_H)}{m_A} \tag{A.9}$$

$$z_A = \frac{(z_H m_H - r_F m_F)}{m_A} \tag{A.10}$$

Mass moments of inertia for the front assembly:

$$I_{Axx} = I_{Hxx} + I_{Fxx} + m_H(z_H - z_A)^2 + m_F(z_F - z_A)^2 \tag{A.11}$$

$$I_{Axz} = I_{Hxz} - m_H(x_H - x_A)(z_H - z_A) + m_F(w - x_A)(r_F + z_A) \tag{A.12}$$

$$I_{Azz} = I_{Hzz} + I_{Fzz} + m_H(x_H - x_A)^2 + m_F(w - x_A)^2 \tag{A.13}$$

Center of mass of the front assembly:

$$u_A = (x_A - w - c)cos(\lambda) - z_A sin(\lambda) \tag{A.14}$$

Mass moments and products of inertia about the steer axis and the skewed axises.

$$I_{A\lambda\lambda} = m_A(u_A)^2 + I_{Axx}(sin(\lambda))^2 + 2I_{Axz}sin(\lambda)cos(\lambda)I_{Azz}(cos(\lambda))^2 \tag{A.15}$$

$$I_{A\lambda * x} = -m_A u_A z_A + I_{Azz}sin(\lambda) + I_{Axz}cos(\lambda) \tag{A.16}$$

$$I_{A\lambda * z} = m_A u_A x_A + I_{Axz}sin(\lambda) + I_{Azz}cos(\lambda) \tag{A.17}$$

The ratio of the mechanical trail to the wheel base:

$$\mu = \frac{c}{w}cos(\lambda) \tag{A.18}$$

Rear and Front wheel angular momenta along the y-axis:

$$S_R = \frac{I_{Ryy}}{r_R}, \quad S_F = \frac{I_{Fyy}}{r_F}, \quad S_T = S_R + S_F \tag{A.19}$$

$$S_A = m_A u_A + \mu m_T x_T \tag{A.20}$$

A.1 Formation of the Linearized Equations of Motion

The linearized equations of motion for the bicycle model 3.1 matrices $[M]$, $[C_1]$, $[K_0]$, and $[K_2]$ are 2x2 constant matrices, which are functions of the rider and bicycle parameters formed from the mass moments of inertia and mass properties in Appendix A. The matrices will be described in details here. All the equations are referenced from [3]. The mass matrix [M] is described as

$$[M] = \begin{bmatrix} M_{\phi\phi} & M_{\phi\delta} \\ M_{\delta\phi} & M_{\delta\delta} \end{bmatrix} \tag{A.21}$$

The following stiffness matrices include $[K_0]$, $[K_2]$, and $[C_1]$.

$$[K_0] = \begin{bmatrix} K_{0\phi\phi} & K_{0\phi\delta} \\ K_{0\delta\phi} & K_{0\delta\delta} \end{bmatrix} \tag{A.22}$$

$$[K_2] = \begin{bmatrix} K_{2\phi\phi} & K_{2\phi\delta} \\ K_{2\delta\phi} & K_{2\delta\delta} \end{bmatrix} \tag{A.23}$$

$$[C_1] = \begin{bmatrix} C_{1\phi\phi} & C_{1\phi\delta} \\ C_{1\delta\phi} & C_{1\delta\delta} \end{bmatrix} \tag{A.24}$$

Each of these matrices can be described with the defined form equivalences.

Matrices Definition	Defined Form Equivalence
$[M_{\phi\phi}]$	I_{Txx}
$[M_{\phi\delta}]$	$I_{A\lambda*x} + \mu(I_{Txz})$
$[M_{\delta\phi}]$	$M_{\phi\delta}$
$[M_{\delta\delta}]$	$I_{A\lambda*\lambda} + 2\mu(I_{A\lambda*z} + (\mu)^2(I_{Tzz})$
$[K_{0\phi\phi}]$	$m_T z_T$
$[K_{0\phi\delta}]$	$-S_A$
$[K_{0\delta\phi}]$	$[K_{0\phi\delta}]$
$[K_{0\delta\delta}]$	$-S_A sin(\lambda)$
$[K_{2\phi\phi}]$	0
$[K_{2\phi\delta}]$	$\frac{(S_T - m_T z_T)}{w}(cos(\lambda))$
$[K_{2\delta\phi}]$	0
$[K_{2\delta\delta}]$	$\frac{(S_A + S_F sin(\lambda))}{w}(cos(\lambda))$
$[C_{1\phi\phi}]$	0
$[C_{1\phi\delta}]$	$\mu * S_T + S_F * cos(\lambda) + \frac{I_{Txz}}{w}(cos(\lambda)) - \mu * m_T Z_T$
$[C_{1\delta\phi}]$	$-((\mu)S_T + S_F cos(\lambda))$
$[C_{1\delta\delta}]$	$\frac{I_{A\lambda*z}}{w}(cos(\lambda)) + \mu(S_A + \frac{I_{Tzz}}{w}cos(\lambda))$

A.2 Brompton Bicycle Parameters

The Brompton Bicycle Parameters are tabulated below. These parameters are from the Solidworks model 2.1 and table 2.1.

Matrices Definition	Value
$[M_{\phi\phi}^{-1}]$	0.0158
$[M_{\phi\delta}^{-1}]$	-0.3607
$[M_{\delta\phi}^{-1}]$	-0.3607
$[M_{\delta\delta}^{-1}]$	39.1715
$[K_{0\phi\phi}]$	-69.6769
$[K_{0\phi\delta}]$	-0.7634
$[K_{0\delta\phi}]$	-0.7634
$[K_{0\delta\delta}]$	-0.2232
$[K_{2\phi\phi}]$	0
$[K_{2\phi\delta}]$	63.0188
$[K_{2\delta\phi}]$	0
$[K_{2\delta\delta}]$	0.7118
$[C_{1\phi\phi}]$	0
$[C_{1\phi\delta}]$	26.1139
$[C_{1\delta\phi}]$	-0.0885
$[C_{1\delta\delta}]$	0.3999

Appendix B

Additional Formulas

B.1 Frequency Sweep Input Design Equations

Two complete frequency sweep long-period inputs are inserted into the time history data section in FRESPID package. The corresponding period (T_{max}) can be calculated based on your minimum frequency of interest (ω_{min}). The corresponding period can be calculated as [4],

$$T_{max} = \frac{2\pi}{\omega_{min}} \tag{B.1}$$

The corresponding period (T_{min}) can be calculated based on your maximum frequency of interest (ω_{max}). The corresponding period can be calculated as [4],

$$T_{min} = \frac{\omega_{max}}{2\pi} \tag{B.2}$$

The data record length for a single sweep should be five times the T_{max} [4].

B.2 Cost Function Equations

The cost function for n_{TF} transfer functions includes a common number of frequency points n_w. The following equation describes the cost function [4],

$$J = \sum_{l=1}^{n_{TF}} \left\{ \frac{20}{n_w} \sum_{\omega_1}^{\omega_{n_\omega}} W_\gamma [W_g(|\hat{T}_c| - |T|)^2 + W_p(< \hat{T}_c - < T)^2] \right\}_l \tag{B.3}$$

where,

| | = magnitude (dB) at each frequency ω

$<$ = phase (deg) at each frequency ω

n_ω = number of frequency points

ω_1 and ω_{n_ω} = starting and ending frequencies of fit

The average cost function is [4],

$$J_{ave} = \frac{J}{n_{TF}} \tag{B.4}$$

B.3 Determining the Cramer-Rao Bounds Equations

The Cramer-Rao bound of the ith identified parameter of the converged solution is Θ_0 is determined from the diagonal element of the inverse of the Hessian matrix H [4]:

$$CR_i \;=\; \sqrt{(H^{-1})_{ii}} \tag{B.5}$$

where the (n_p x n_p) matrix H is defined as

$$H \;=\; \nabla^2_\Theta J \;=\; \frac{\partial^2 J}{\partial\Theta\partial\Theta^T} \;=\; \begin{bmatrix} \frac{\partial^2 J}{\partial\theta_1^2} & \frac{\partial^2 J}{\partial\theta_1\partial\theta_2} & \cdots & \frac{\partial^2 J}{\partial\theta_1\partial\theta_{n_p}} \\ \frac{\partial^2 J}{\partial\theta_2\partial\theta_1} & \frac{\partial^2 J}{\partial\theta_2^2} & \cdots & \frac{\partial^2 J}{\partial\theta_2\partial\theta_{n_p}} \\ & & \cdots & \\ \frac{\partial^2 J}{\partial\theta_{n_p}\partial\theta_1} & \frac{\partial^2 J}{\partial\theta_{n_p}\partial\theta_2} & \cdots & \frac{\partial^2 J}{\partial\theta_{n_p}^2} \end{bmatrix} \tag{B.6}$$

where, J represents the cost function B.3. Additional information can be found in [4].

B.4 Time Verification Model Equations

When estimating the residual bias ($\dot{x_b}$) and the reference-shift y_{ref} vectors are collected into one vector called the identification parameter (Θ). The following equations are referenced from [4] this describes the cost function (J), *rms fit error*, and includes the *Theil inequality coefficient (TIC).*

$$J(\Theta) \;=\; \sum_{i=1}^{n_t}[(y_{data} - y)^T W (y_{data} - y)] \tag{B.7}$$

where, y_{data} is the perturbation time-history vector from the verification flight data. y is the perturbation model time-history response vector obtained (5.28) from the integration of the model equations. n_t is the number of time-history points in the verification data record. W is the diagonal matrix of the weighting factors for each output

$(n_0 \ x \ n_0)$. The weighting factors W equation includes,

$$W \ = \ diag\left\{wt_{y1}^2, wt_{y2}^2, ..., wt_{y_{n_0}}^2\right\} \tag{B.8}$$

For many applications a good choice in choosing your units include the following,

$$1deg - error \ : \ 1deg/s - error \ : \ 1ft/s - error \ : \ 1ft/s^2 - error \tag{B.9}$$

If the above units were not used in any of the CIFER software, a set of weights must be used. The weight conversion are from degrees to radians (57.3).

The *rms fit error* is expressed as

$$J_{rms} = \sqrt{\frac{1}{(n_t \cdot n_{0)}} \sum_{i=1}^{n_t} [(y_{data} - y)^T W (y_{data} - y)]} \tag{B.10}$$

The J_{rms} provides a useful overall measure of model time-domain accuracy [4]. The *Theil inequality coefficient (TIC)* equation includes the weighting (B.8) equation from above.

$$TIC \ = \ \frac{\sqrt{\frac{1}{(n_t \cdot n_{0)}} \sum_{i=1}^{n_t} [(y_{data} - y)^T W (y_{data} - y)]}}{\sqrt{\frac{1}{(n_t \cdot n_{0)}} \sum_{i=1}^{n_t} [y^T W y]]} + \sqrt{\frac{1}{(n_t \cdot n_{0)}} \sum_{i=1}^{n_t} [y_{data}^T W y_{data}]}} \tag{B.11}$$

B.5 Linear Quadratic Regulation Formulas

The following equations describe the LQR problem [8],

$$J_{LQR} := \int_0^\infty \|z(t)\|^2 + p\|u(t)\|^2 dt \tag{B.12}$$

where, p is a positive constant. The term

$$\int_0^\infty \|z(t)\|^2 dt \tag{B.13}$$

correspond to the energy controlled output and the term

$$\int_0^\infty \|u(t)\|^2 dt \tag{B.14}$$

corresponds to the energy of the control signal. By using the LQR equation we can minimize both of these energies.